

# Assessment of Abrupt Shifts in CMIP6 Models using Edge Detection

Sjoerd Terpstra<sup>a,b,✉</sup>, Swinda K.J. Falkena<sup>a</sup>, Robbin Bastiaansen<sup>a,c</sup>, Sebastian Bathiany<sup>d,e</sup>, Henk A. Dijkstra<sup>a,b</sup>, and Anna S. von der Heydt<sup>a,b</sup>

<sup>a</sup>Institute for Marine and Atmospheric research Utrecht, Utrecht University, Utrecht, The Netherlands

<sup>b</sup>Centre for Complex Systems Studies, Utrecht University, Utrecht, The Netherlands

<sup>c</sup>Mathematical Institute, Utrecht University, Utrecht, The Netherlands

<sup>d</sup>Earth System Modelling, School of Engineering and Design, Technical University of Munich, Munich, Germany

<sup>e</sup>Potsdam Institute for Climate Impact Research, Potsdam, Germany

Research over the past decade has shown that multiple elements of the climate system, such as the Arctic Winter sea ice or the Amazon rainforest, could undergo abrupt shifts, but there are large uncertainties regarding their timing and spatial extent. In this study we investigated when and where abrupt shifts occur in the latest generation of climate models (CMIP6) under a scenario of a 1% annual increase in CO<sub>2</sub>. We considered 82 ocean, atmosphere, and land variables across 57 models. We used a Canny edge detection method—adapted for spatiotemporal dimensions—to detect abrupt shifts occurring on time scales from years to decades. Then, we performed a connected component analysis to quantify the spatial extent of these shifts. The systems analyzed include the North Atlantic subtropical gyre, Tibetan Plateau, land permafrost, Amazon rainforest, Antarctic sea ice, monsoon systems, Arctic summer sea ice, Arctic winter sea ice, and Barents sea ice. With the exception of the monsoons systems, we found abrupt shifts in multiple models per system. We observed a considerable variation across the different CMIP6 models in terms of timing and spatial extent. Higher levels of global warming increased the risk of abrupt shifts in CMIP6 models. Even at a global warming level of 1.5 °C, six out of ten studied climate subsystems showed abrupt shifts that cover a substantial area in multiple models.

CMIP6 | Tipping element | Abrupt shift | Abrupt change | Climate

Correspondence: [s.terpstra@uu.nl](mailto:s.terpstra@uu.nl)

Due to increasing levels of greenhouse gases, the climate is changing rapidly, bringing about negative consequences such as loss of biodiversity (1, 2), rising sea level (3), and more numerous extreme events (4). Additionally, there is concern that this increase in greenhouse gases could lead to large and sudden changes in the climate system known as abrupt shifts. An abrupt shift is defined as “a change that takes place substantially faster than the rate of change in the recent history of the affected component of a system” according to the most recent IPCC report (5, p. 202). A related concept is that of a tipping point (6, 7) defined as “a critical threshold beyond which a system reorganizes, often abruptly and/or irreversibly” (5, p. 202). Crossing a tipping point can lead to an abrupt shift when a system reorganizes in a sudden manner. However, tipping dynamics can also occur over much longer timescales compared to the internal dynamics of these systems—and thus does not have to be abrupt. In this paper, we focus on abrupt shifts in which a system changes faster than expected compared to its recent history.

Abrupt shifts have been found in many climate models of

different complexity (8–10). The potential for abrupt shifts is further supported by evidence from paleoclimate, such as the recurring abrupt shifts during Dansgaard-Oeschger events (11). During these events, rapid warming occurs on a timescale of decades, likely linked to abrupt changes in sea ice cover and the Atlantic Meridional Overturning Circulation (AMOC) (12, 13). Since such sudden changes can have large impacts on ecosystems and society (14, 15), predicting them with good accuracy is crucial.

Yet, there are large uncertainties surrounding abrupt shifts. For example, it is unclear under which conditions—such as under which critical forcing thresholds—climate subsystems undergo abrupt shifts (6, 7, 16, 17). Efforts to reduce these uncertainties include the work by Drijfhout et al. (18) on abrupt shifts in a recent generation of earth system models (CMIP5) (19). In Drijfhout et al. (18), all CMIP5 models were scanned for abrupt shifts in simulations of potential future climates. The authors found evidence of abrupt shifts in a variety of systems and demonstrated that most of them had a limited spatial extent, with the majority involving ocean-sea ice interactions.

While the results of Drijfhout et al. (18) advanced our understanding of abrupt shifts, the downside of their method was that it involved manual steps. To improve the detection of abrupt shifts in climate data, Bathiany et al. (20) adapted the Canny edge detection method (21)—typically used in computer vision—for usage with climate data. This method detects edges, which are points in space and time where abrupt changes occur. Hence, it is possible to automatically detect abrupt shifts in climate data. The authors used this method to scan the same CMIP5 models as Drijfhout et al. (18). Both studies highlighted similar results, with the highest fraction of abrupt shifts detected in polar regions, mostly in the Northern Hemisphere. While Bathiany et al. (20) validated the edge detection method on the CMIP5 models, their study was limited to a general scan of abrupt shifts where they only counted the number of abrupt shifts on the grid cell level per variable. They did not quantify global warming thresholds at which these shifts occur, nor did they analyze the spatial extent of abrupt shifts.

Recognizing the usefulness of edge detection, we apply it to the current state-of-the-art climate models (CMIP6) which have not yet been thoroughly subjected to a scan for abrupt shifts. The CMIP6 models are the latest generation of fully

coupled earth system models (22) used as a basis for the IPCC reports. For this study, we consider the standard 1pctCO2 simulation of CMIP6. This is a simulation over 150 years in which the CO<sub>2</sub> concentration is increased annually by 1% until the CO<sub>2</sub> levels are four times the preindustrial levels at 140 years in the simulation. We use 82 two-dimensional land, ocean, and atmosphere variables such as vegetation, sea ice, and temperature fields (see Table S2 for the full list). The strength of this study lies in determining the global warming thresholds and spatial extent of abrupt shifts using edge detection on the updated CMIP6 models, which offer a better representation of physical processes compared to the CMIP5 models.

We investigate abrupt shifts occurring in different climate subsystems whose physical dynamics are well-represented within the CMIP6 models, structuring our analysis based on the overview provided by the recently published Global Tipping Points Report (GTP) (17). This report synthesizes current evidence for tipping dynamics in various earth system components. It ranks climate subsystems as tipping elements, unclear tipping elements, or not tipping elements based on their plausibility of possessing tipping points.

Our analysis is limited to time scales of decades or shorter. We do not examine subsystems with longer timescale dynamics since the 1pctCO2 scenario spans only 150 years and systems like ice sheets are not well-represented in the models. Moreover, we focus on abrupt shifts, which may be harder to adapt to, rather than long-term processes. For example, while the collapse of the Greenland ice sheet would have extreme consequences for the climate system, this transition could occur over a timescale much longer than human lifespans and might even be reversible (23), whereas humankind may fail to adapt to faster collapses, such as the sudden loss of rainforests.

Based on these considerations, we analyze all climate subsystems that are adequately represented in CMIP6 and have the potential for abrupt shifts under the 1pctCO2 scenario (see SI Text S1.E for a detailed justification of the included systems). Of the subsystems identified as tipping elements with low to high confidence in the GTP (17), we analyze the North Atlantic subpolar gyre, the Tibetan Plateau, the land permafrost in the Northern Hemisphere, the Amazon rainforest, and the Boreal forests. Of the subsystems identified as unclear tipping elements, we analyze the Indian, West African and South American Monsoons, and the Antarctic sea ice. Finally, for subsystems identified as not tipping elements, we consider the Arctic summer sea ice, the Arctic winter sea ice, and the Barents sea ice. Although these last three subsystems are not classified as tipping elements, they still exhibit abrupt transitions in CMIP5 models (18, 20).

To distinguish between minor fluctuations and actual abrupt shifts on a timescale of a decade, we apply an abruptness measure adapted from Bathiany et al. (20). This measure quantifies the amplitude of the detected shift relative to the typical variance of the variable (measured from a control simulation with CO<sub>2</sub> concentration fixed at preindustrial levels) to classify a change only as an abrupt shift if the amplitude of

change is large enough (See *Material and Methods* for more details). After applying the edge detector, we use a connected component algorithm to connect all edges to determine regions that show abrupt shifts simultaneously, enabling us to separate small- and large-scale abrupt shifts in climate subsystems. In the rest of this paper, by an abrupt shift we mean the full connected component experiencing an abrupt shift except when stated otherwise. A large-scale abrupt shift is defined as covering an area of more than a given threshold unique for each system. We link the spatially detected abrupt shifts to the level of global warming at which they occur in the models.

## Results

**Global analysis of abrupt shifts in CMIP6.** Figure 1 shows a global overview of detected abrupt shifts in the CMIP6 model ensemble. The heat map in Figure 1A denotes the fraction of models that have at least one abrupt shift per grid cell in any month in any variable. Certain climate subsystems experience more abrupt shifts than others; especially the polar regions exhibit many abrupt shifts on the level of grid cells. The boxes indicate the different climate subsystems we have analyzed in this study (except for the monsoons, see figure caption). See Table 1 for an overview of these systems, their coordinates, key variables, and area thresholds we have chosen to define large-scale abrupt shifts in each subsystem.

To give an impression of how these large-scale abrupt shifts look like, example time series of these shifts are shown in Figure 2 for each climate subsystem. By aggregating the large-scale abrupt shifts from all models and all key variables in each subsystem, we obtained a distribution of the global warming level at which these shifts occur. Figure 1B shows these distributions per climate subsystem together with the estimated temperature thresholds by McKay et al. (6).

There is a large difference in the number of abrupt shifts between CMIP6 models. There are 9 models without any large-scale abrupt shifts in any of the climate subsystems (large-scale: abrupt shifts covering at least the area given in Table 1 for each subsystem). 48 models have at least one large-scale abrupt shift in any subsystem. The majority of models (39) have between 2 and 4 subsystems with a large-scale abrupt shift. There are 3 models with 5 or more subsystems exhibiting large-scale abrupt shifts. Figure S5 and Table S3 summarize the subsystems and variables with abrupt shifts per model.

To test if the number of abrupt shifts in a model depends on its climate sensitivity, we performed a two-sided Pearson correlation test between the number of subsystems with large-scale abrupt shifts per model with the models' transient climate response (TCR, model values obtained from (5, 24)). The TCR is defined as the level of global warming after 70 years from a 1% annual increase in CO<sub>2</sub> starting from preindustrial conditions until CO<sub>2</sub> doubling. We excluded the Amazon rainforest and Boreal forests as no consistent signals were detected (see the Amazon Rainforest and Boreal Forests sections). The correlation between TCR and the num-

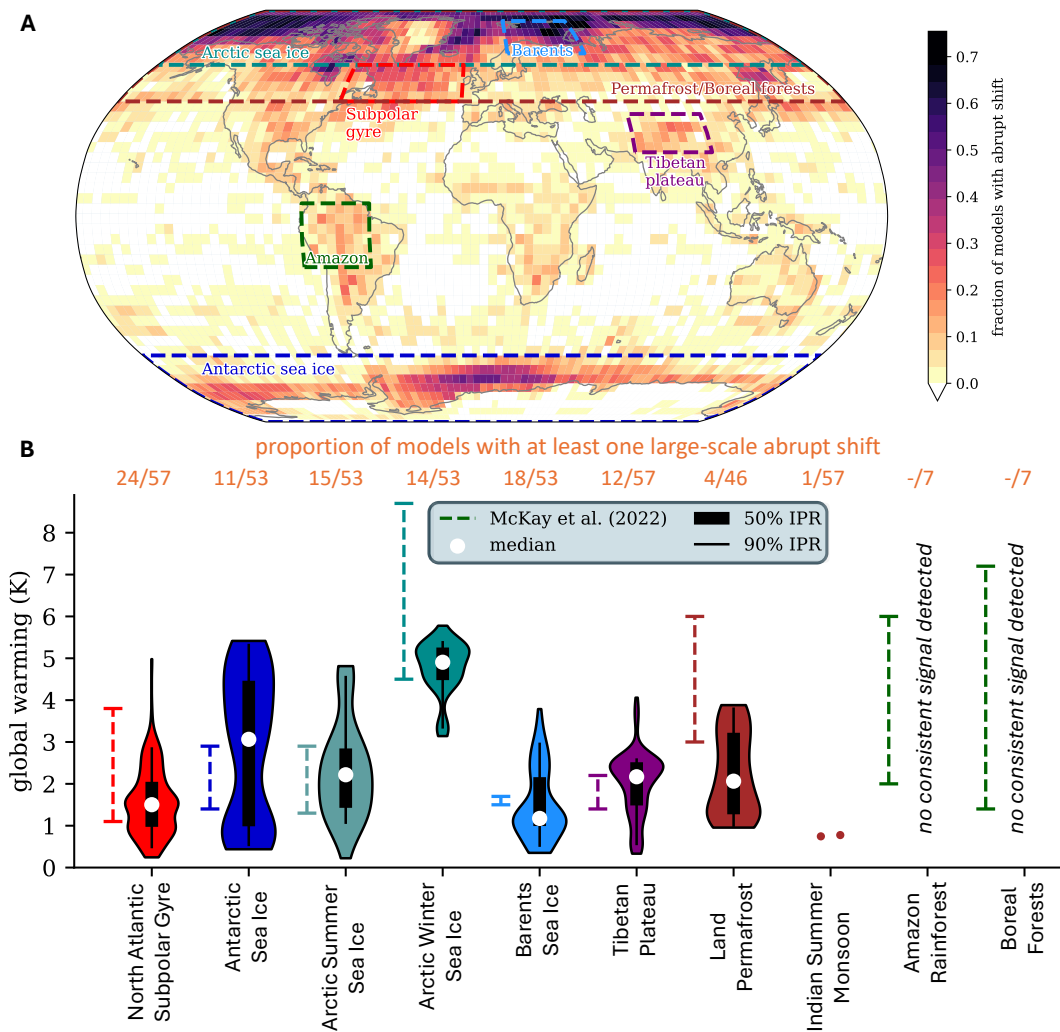


**Fig. 1. (A) Fraction of models that have an abrupt shift per grid cell in at least one of the 82 tested variables.** This is based on the abrupt shifts at a grid cell level. Highlighted are the different systems of focus in this paper; tipping elements: North Atlantic subpolar gyre, Tibetan Plateau, Land permafrost, Amazon rainforest, Boreal forests; unclear tipping elements: Antarctic sea ice, Monsoons; not tipping elements: Arctic summer sea ice, Arctic winter sea ice, Barents sea ice. The boxes for the monsoons are not drawn, but they include the South American Monsoon, West African Monsoon, and Indian Summer Monsoon. **(B) The mean global temperature increase at which large-scale abrupt shifts are detected in different climate subsystems.** Each violin plot illustrates the normalized density distribution of global warming at which large-scale abrupt shifts are detected across all models for the key variables relevant to each subsystem (see Table 1). A large-scale abrupt shift is defined as one covering a surface area exceeding a specific threshold, as detailed in Table 1 for each subsystem. The white dots show the mean, the thick black lines show the 50% interpercentile range (IPR), and the thin black lines the 90% IPR. For the Indian Summer Monsoon only two instances of abrupt shifts are found, these are denoted by the two dots. Also displayed is the proportion of models that have a large-scale abrupt shift per subsystem. The dashed lines show the global warming thresholds as estimated by McKay et al. (6) if available.

ber of subsystems with large-scale abrupt shifts is  $r = 0.532$  with  $p = 0.001$ , meaning a significant correlation of moderate positive strength. Thus, models with high TCR generally have more large-scale abrupt shifts than models with low TCR. In the 1pctCO<sub>2</sub> scenario, high TCR models experience greater warming, making abrupt shifts more likely in subsystems with high temperature thresholds such as Antarctic sea ice. The correlation with the equilibrium climate sensitivity (ECS) is also significant with a moderate positive strength (SI Text S2.A).

In the next subsections, we analyze each climate subsystem individually. We first look at subsystems identified as tipping elements, then at subsystems identified as unclear tipping elements, and last at subsystem identified as not tipping elements.

### Subsystems identified as tipping elements.

**North Atlantic subpolar gyre.** In the North Atlantic subpolar gyre, ocean convection occurs. The sinking of dense waters in this region contributes to the AMOC. The subpolar gyre is identified as a separate tipping element from the AMOC and a collapse of convection is expected to occur abruptly with medium confidence (17). As evidence for a collapse, we expect to find negative abrupt shifts—defined as abrupt declines—in the sea surface salinity, the mixed layer depth, the sea surface temperature and—related to the latter—the surface air temperature.

In total, 24 out of 57 models show an abrupt shift in the subpolar gyre for the sea surface salinity, the mixed layer depth, the sea surface temperature, or the surface air temperature. The surface air temperature has been used in a previous study

**Table 1.** Overview of the analyzed climate subsystems. The table shows the latitude and longitude bounds, the key variables (which are the focus of the analysis), and the minimum area required for an abrupt shift to be considered large-scale for each subsystem ('-' means there is no minimum area threshold).

	Latitude	Longitude	Key variables	Minimum Area (km <sup>2</sup> )
<b>Subsystems identified as tipping elements</b>				
North Atlantic subpolar gyre	(45, 60)	(-70, -10)	mixed layer depth, sea surface salinity, sea surface temperature, surface air temperature	-
Tibetan Plateau	(25, 40)	(70, 105)	snow area percentage, surface snow melt, snow depth, near-surface air temperature, surface upwelling shortwave radiation	10 <sup>5</sup>
Land permafrost	(45, 90)	(-180, 180)	soil frozen water content, total soil moisture content	10 <sup>6</sup>
Amazon rainforest	(-20, 5)	(-80, -50)	bare soil percentage area coverage, carbon mass in vegetation, carbon mass in soil pool, carbon mass flux into atmosphere due to fire, total carbon mass flux from vegetation to litter/from vegetation directly to soil	-
Boreal forests	(45, 80)	(-180, 180)	carbon mass flux out of atmosphere due to gross primary production on land, natural grass area percentage, leaf area index, total atmospheric respiration on land as carbon mass flux, tree cover percentage	-
<b>Subsystems identified as unclear tipping elements</b>				
Antarctic sea ice	(-90, -55)	(-180, 180)	sea ice concentration, sea ice thickness, sea-ice mass change through bottom melting & surface melting, surface upwelling shortwave radiation, near-surface air temperature	5 · 10 <sup>5</sup>
South American Monsoons: West African Indian Summer	(-20, 5) (-20, 5) (-20, 5)	(-80, -50) (-80, -50) (-80, -50)	precipitation, convective precipitation, latent heat flux	-
<b>Subsystems identified as not tipping elements</b>				
Arctic summer & winter sea ice	(60, 90)	(-180, 180)	sea ice concentration, sea ice thickness, sea-ice mass change through bottom melting & surface melting, surface upwelling shortwave radiation, near-surface air temperature	10 <sup>6</sup>
Barents sea ice	(65, 81)	(15, 60)	sea ice concentration, sea ice thickness, sea-ice mass change through bottom melting & surface melting, surface upwelling shortwave radiation, near-surface air temperature	2 · 10 <sup>5</sup>

to identify abrupt shifts in the subpolar gyre (10). For this variable we find 7 models with an abrupt shift, which occur between 0.31 and 2.03 K of global warming (90% IPR (interpercentile range)). For sea surface temperature, 22 models show an abrupt shift. All but one (CNRM-CM6-1-HR) of the models with an abrupt shift in surface air temperature also show an abrupt cooling in sea surface temperature. There are thus more abrupt shifts in sea surface temperature than in surface air temperature. This difference may result from a damping effect, where the cooling of the atmosphere is less pronounced compared to the cooling of the ocean surface. The sea surface temperature shifts occur between 0.49 and 2.99 K of global warming (90% IPR).

For observing convection, the mixed layer depth is the most suitable variable because it provides a more direct measure of convection than surface temperatures. 11 models show an abrupt shift in the mixed layer depth, of which 10 also exhibit an abrupt cooling of sea surface temperature (only IPSL-CM5A2\_INCA does not). The abrupt shifts in mixed layer depth occur between 0.47 and 2.14 K of global warming (90% IPR). On average they cover at most a few grid cells, which is to be expected since convection is a local process. Figure 2A shows an example of such an abrupt shift in the mixed-layer depth in MRI-ESM2-0. Lastly, for sea surface salinity, 2 models show an abrupt shift, both over reasonably large areas. These models are BCC-ESM1 (occurring at 0.97 K of global warming, with the area being at least  $5.7 \cdot 10^5$  km<sup>2</sup>) and CESM2-FV2 (occurring at 1.35 K of global warming, with the area being at least  $9.8 \cdot 10^5$  km<sup>2</sup>). The locations of the abrupt shifts do not happen at consistent locations and seem highly model-dependent.

In CMIP5, 5 models were found to show abrupt shifts in the Labrador sea related to convection (18). Here, we identify 19 models as having abrupt shifts in the subpolar gyre. The risk of abrupt shifts in the subpolar gyre region has also been assessed by Swingedouw et al. (10) for CMIP6, where they considered the average surface air temperature over a box covering the subpolar gyre region instead of grid cell data as is done here. For 2 of the 3 models for which they identify abrupt shifts (CESM2-WACCM, MRI-ESM2-0), we

also detect abrupt shifts. Using the edge detection method no abrupt shifts are found for the third model (NorESM2-LM). This can be due to the different model scenarios used (here 1pctCO2, Swingedouw et al.(10) used the Shared Socio-Economic Pathways (SSPs) (25, 26)). The high global mean temperature increase in the 1pctCO2 scenario offsets part of the cooling caused by a subpolar gyre collapse, which could lead to missing some events in sea surface and surface air temperatures. Still, we detect more abrupt shifts in the sea surface temperature than in the mixed layer depth, likely because the high variability in the latter makes it difficult to distinguish abrupt shifts from natural fluctuations.

**Tibetan Plateau.** Glaciers outside the large polar ice masses can exhibit complicated nonlinear dynamics, mostly driven by (local) surface air temperature changes. Therefore, the world's glaciers including those on the Tibetan Plateau have been classified as regional tipping elements (medium confidence) (17). While glacier dynamics are not resolved in the CMIP6 models considered here, the snow cover on such glaciers can be assessed. In CMIP5, two models experienced abrupt decline of the snow cover in the Tibetan Plateau region (18).

In 12 out of 57 CMIP6 models we find a large-scale abrupt shift in at least one of the key variables (see Table 1). The surface upwelling shortwave radiation, which is affected by the surface albedo, shows the highest proportion of abrupt shifts, with shifts occurring in 11 models between 0.69 and 2.60 K of global warming (90% IPR). An abrupt decline in albedo is most likely caused by the disappearance of snow cover.

Three variables directly represent the snow cover of the Tibetan Plateau: snow area percentage, surface snow melt, and snow depth. Of these, abrupt shifts in snow depth occur at the lowest level of global warming between 0.36 and 2.61 K (90% IPR) in 7 models. Abrupt shifts in snow area percentage occur between 1.41 and 3.59 K (90% IPR, 5 models) and for surface snow melt between 1.90 and 3.82 K (90% IPR, 2 models). The models with abrupt shifts in these last two variables are subsets of the models with detected shifts in snow

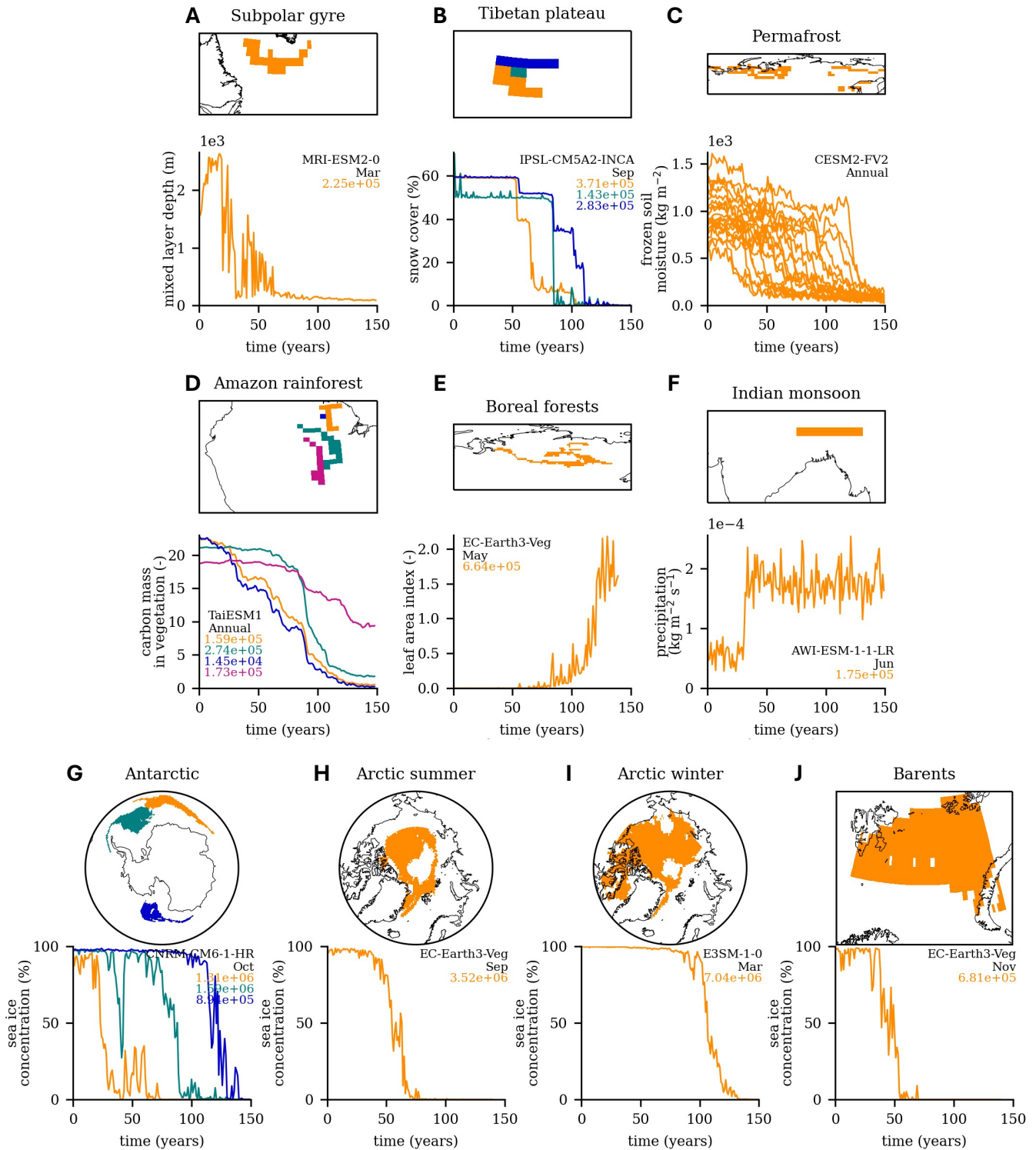


**Fig. 2.** The spatial extent and time series of a large-scale abrupt shift for a representative variable and model is shown for each of (A) North Atlantic subpolar gyre, (B) Tibetan Plateau, (C) Amazon rainforest, (D) Boreal forests, (E) Land permafrost, (F) Indian summer Monsoon, (G) Antarctic sea ice, (H) Arctic summer sea ice, (I) Arctic winter sea ice, and (J) Barents sea ice. In each panel, the model and month in which the abrupt shift(s) occur are denoted (where 'Annual' indicates a yearly average instead), with the surface area covered by the abrupt shift(s) shown in the same color as each time series in  $\text{km}^2$ . The spatial plots are located within the boxes of Figure 1A. The Boreal forest and land permafrost subsystems are zoomed into regions of Northern Asia. The Indian summer monsoon example is located south of the Tibetan plateau.

depth. This indicates that snow depth declines abruptly before the surface snow melts (since the abrupt shifts in snow depth occur at a lower level of global warming than in snow area percentage and surface snow melt). Finally, we find 4 models (of which 3 are versions of the CanESM5 model) that

have an abrupt shift in near-surface air temperature between 1.19 and 2.52 K of global warming (90% IPR). Figure 2B shows the abrupt decline of snow area percentage in IPSL-CM5A2-INCA.

Overall, only 12 models out of 57 show an abrupt shift in

snow-related variables in the CMIP6 models spread over a limited area. However, since glacier dynamics are not resolved in the CMIP6 models, the number of abrupt shifts in the Tibetan Plateau might be underestimated because abrupt shifts in the glaciers themselves cannot be represented.

**Land Permafrost.** In the GTP (17), the land permafrost areas in the Northern Hemisphere are classified as regional tipping elements (medium confidence), while, on a global scale, permafrost-related processes are not considered to have tipping potential with medium confidence. Abrupt thaw of permafrost occurs through processes such as thermokarst formation, leading to subsiding ground and rapid expansion of thaw lakes (27). Without these nonlinear processes, permafrost thaw is considered more gradual. On a global scale, the positive carbon-climate feedback (extra CO<sub>2</sub> and methane emissions from soil degradation after thaw) could make land permafrost a tipping element. However, this feedback is currently considered too small to be important globally (17), and the simulations considered here do not include it because they are driven by prescribed CO<sub>2</sub> concentrations. Despite this, Drijfhout et al. (18) did find one CMIP5 model exhibiting an abrupt change in total soil moisture content, indicating an abrupt melt of permafrost in the Arctic tundra. Apart from the total soil moisture content, we focus our analysis on the soil frozen water content, as this is a proxy for permafrost (28).

Both total soil moisture content and soil frozen water content show abrupt shifts in the CMIP6 models. However, there is a large difference between the two variables in the fraction of positive abrupt shifts (i.e., abrupt increase) and negative abrupt shifts (i.e., abrupt decrease). Figure 3 shows the number of positive and negative abrupt shifts detected over all models for frozen soil moisture content (panel A) and total soil moisture content (panel C) depending on the area these shifts cover. For total soil moisture content, there are many positive as well as negative shifts (Figure 3C). However, for abrupt shifts covering more than 1 million km<sup>2</sup>, there are only negative ones with 4 out of 46 models exhibiting a large-scale negative abrupt shift (between 0.95 and 3.84 K of global warming (90% IPR)).

In contrast to total soil moisture content, soil frozen water content shows a considerably higher number of negative (i.e., abrupt decline) than positive abrupt shifts (i.e., abrupt increase), most of which are small shifts (Figure 3A). Just one model shows large-scale negative abrupt shifts covering an area of at least 1 million km<sup>2</sup> each (UKESM1-0-LL). There are 36 separate instances of abrupt shifts in this model that occur between 1.17 and 3.27 K of global warming (90% IPR). Figure 2C shows all abrupt declines in CESM2-FV2 in Northern Asia for the annual time series for soil frozen water content.

However, since permafrost is expected to be a regional tipping point, we have also looked at the total area of all abrupt shifts in a simulation (i.e., the total area of abrupt shifts in a single month or year) which is displayed in Figure 3B&D for both positive and negative shifts. For frozen soil moisture, there are 19 out of 36 models with negative abrupt shifts covering a total area of at least 1 million km<sup>2</sup>, with the largest total area being  $6.3 \cdot 10^6$  km<sup>2</sup>. For total soil moisture content, in 8 models the abrupt shifts cover a total area of at least 1 million km<sup>2</sup>.

In summary, we find abrupt shifts in frozen soil moisture content. However, individual abrupt shifts are small (covering an area of less than 1 million km<sup>2</sup>) except for 1 model. Taking into account the total area of abrupt shifts in a single simulation, we find that, with 19 models, permafrost can still disappear abruptly on a regional scale.

**Amazon Rainforest.** The Amazon rainforest is considered a tipping element by the GTP (17). The report evaluates the tipping potential of this element with high confidence at the local scale, medium confidence at the regional scale, and low confidence at the continental scale. Shifts at all three scales are expected to occur abruptly with medium confidence.

In our assessment, we only consider the seven CMIP6 models that have dynamic vegetation. These are EC-Earth3-Veg, GFDL-ESM4, MPI-ESM1-2-LR, NorCMP1, TaiESM1, SAM0-UNICON, and UKESM1-0-LL. Among these, EC-Earth3-Veg, GFDL-ESM4, MPI-ESM1-2-LR, and NorCMP1 also simulate fire. We detect many abrupt shifts, most of which are localized events. However, some of the considered variables, such as carbon mass, have low interannual variability, such that the computed abruptness measure detects abrupt shifts that are very small in magnitude. Moreover,

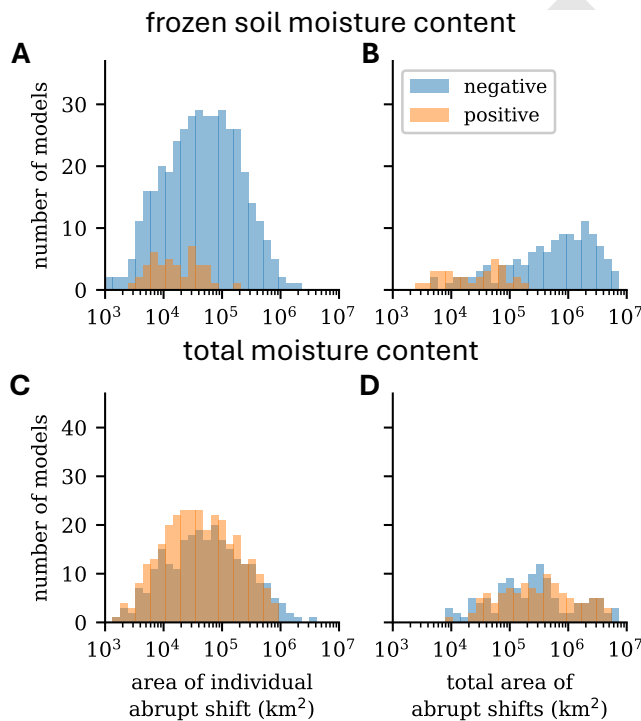


**Fig. 3. Number of models showing abrupt shifts in frozen soil water content and total soil moisture content for land permafrost, depending on the area they cover.** Panels (A) and (C) show the number of models as a function of the area covered by individual abrupt shifts in any month, distinguishing between positive (increase, orange) and negative (decrease, blue) shifts for frozen soil moisture content and total soil moisture content, respectively. Panels (B) and (D) show a similar distribution, but now for the total area affected by these shifts in each month for frozen soil moisture content and total soil moisture content, respectively.

the timescale of vegetation dynamics is generally slower (decades) than in the subsystems we analyzed previously, which is why the edge detector is not optimally configured. Abrupt shifts within CMIP6 models were also analyzed by Parry et al. (29) under the 1pctCO2 scenario. They scanned for abrupt shifts in carbon mass in vegetation using specific criteria: the vegetation carbon must change by at least  $2 \text{ kg C m}^{-2}$  over a 15-year period, contributing to at least 25% of the overall change, with the mean annual rate of change being at least three times larger than the variability in the control run. Their analysis revealed abrupt shifts in all models except for UKESM1-0-LL. These abrupt shifts were mostly localized but added up to between 0 and 40% of total area in the northern South America region of the Amazon at 3 K of global warming.

When we apply a similar additional criterion, requiring at least a 25% increase or decrease up to 30 years before and after the abrupt shift (using the same parts of the time series as for the abruptness measure, see *Materials and Methods*), we still detect abrupt shifts in (number of models with abrupt shift in parentheses) bare soil percentage area coverage (1), carbon mass in vegetation (3), total carbon mass flux from vegetation to litter (1), carbon mass flux out of atmosphere due to gross primary production on land (3), natural grass area percentage (2), leaf area index (3), total atmospheric respiration on land as carbon mass flux (2), and tree cover percentage (2). These abrupt shifts occur between 0.85 and 4.95 K of global warming (90% IPR), and regard relatively small areas. Figure 2D shows an example of abrupt shifts in TaiESM1.

**Boreal Forests.** In the GTP (17), (Northern Hemisphere) Boreal forest changes have been classified as tipping elements on the regional scale (dieback on the southern edge with medium confidence, expansion on the Northern edge with low confidence). As for the Amazon rainforest, we assess abrupt shifts in the subset of CMIP6 simulations that include dynamic vegetation. Suggested drivers of such abrupt changes are regional drying and atmospheric warming, which could potentially be related to permafrost thaw. Southern dieback refers to a tipping point that leads to an almost treeless state (steppe/prairie), while Northern expansion could be an abrupt expansion of tree cover into previously tundra or little vegetated areas. In Drijfhout et al. (18), the abrupt northward expansion of Boreal forests has been observed in two CMIP5 models.

Although considered abrupt, forest expansion still occurs on time scales of more than a decade, making it challenging to detect with the edge detector within the short time series of the 1pctCO2 scenario and the chosen parameters of the edge detector as discussed in the previous section on the Amazon rainforest. We apply the same extra condition (at least 25% increase or decrease up to 30 years period before and after the abrupt shift) here, and find abrupt shifts in (number of models with abrupt shift in parentheses) bare soil percentage area coverage (2), carbon mass in vegetation (2), total carbon mass flux from vegetation to litter (1), total carbon mass flux from vegetation to soil (1), carbon mass flux out

of atmosphere due to gross primary production on land (5), natural grass area percentage (3), leaf area index (4), total atmospheric respiration on land as carbon mass flux (2), and tree cover percentage (2). These abrupt shifts occur between 0.80 and 4.87 K of global warming (90% IPR) and include mostly northward expansion. Figure 2E shows an example of an abrupt increase of leaf area index for EC-Earth3-Veg. Overall, we find some abrupt shifts occurring in the Boreal forests, however, more targeted analysis is necessary to quantify and understand these transitions in CMIP6 models in more detail.

### Subsystems identified as unclear tipping elements.

**Monsoons.** In the GTP (17), only the West African Monsoon is categorized as a tipping element, but with low confidence. For the Indian Summer Monsoon and the South American Monsoon it is unclear whether they are tipping elements. For the Indian Summer Monsoon transitions have been found in proxy data, i.e. cave records (30), where large changes in precipitation are associated with changing monsoon intensity. The suggested main mechanism behind possible tipping is the moisture-advection feedback, where increased precipitation leads to increased latent heating, causing an increased land-ocean temperature difference and hence landward advection of moisture, amplifying the precipitation perturbation (31). We focus the analysis on latent heat flux and both general and convective precipitation, which are linked to this mechanism.

We find no abrupt shifts in (convective) precipitation related to the South American Monsoon and West African Monsoon. For the Indian Summer Monsoon, we find two models with abrupt shifts in precipitation. In one model, AWI-ESM-1-1-LR, an abrupt increase in precipitation is detected in both June and August (see Figure 2F). The abrupt shifts are located close to the Himalaya (covering an area of  $1.5$  and  $1.7 \cdot 10^5 \text{ km}^2$  for the two months). This might be a slight northward shift of the Indian Monsoon system. In the other model, FGOALS-g3, we detect an abrupt increase in precipitation off the coast of south-east India near the last 20 years of the simulation (see Figure S6). Upon visual inspection, it is not clear whether this is an extreme event or a persisting abrupt shift since the precipitation seems to return to its baseline. There are no abrupt shifts detected in latent heat flux.

Overall, we find very limited evidence of abrupt shifts in the Indian Summer Monsoon system and no evidence of abrupt shifts in the West African Monsoon and the South American Monsoon systems.

**Antarctic Sea Ice.** Antarctic sea ice reaches its minimum extent in February and its maximum extent in September. The GTP (17) classifies Antarctic sea ice as an unclear tipping element, also stating that it is uncertain whether it undergoes abrupt shifts.

We found that 36 out of 53 CMIP6 models show an abrupt shift in sea ice concentration of which only 3 models (CNRM-CM6-1-HR, GISS-E2-1-H, UKESM1-1-LL) show

an abrupt shift covering more than 1 million km<sup>2</sup> (the time series for CNRM-CM6-1-HR is shown in Figure 2G). These 3 models show a large spread in the timing of the shifts, ranging between 0.51K and 4.67K of global warming (90% IPR). Large-scale abrupt shifts covering an area of at least 0.5 million km<sup>2</sup> are more numerous, with 11 models displaying such a shift. Figure 4B shows that all of them—except for one in each of April, May, and Annual—occur between June and November. No large-scale abrupt shifts are observed from December to March. This is likely because there is relatively little sea ice in summer in the Antarctic. GISS-E2-1-H is the only model to show an abrupt shift in April and May (occurring at 1K of global warming). The level of global warming at which the abrupt shifts occur from June to November ranges between 0.54 and 5.41 K (90% IPR).

The detected large-scale abrupt shifts in sea ice concentration occur in two different locations, as Figure 4A illustrates. One is around the Weddell Sea and the other around the Amundsen and Ross Seas. In the Weddell Sea the abrupt shifts in sea ice concentration occur between 0.58 and 5.23 K of global warming (90% IPR), and around the Amundsen and Ross Sea between 2.51 and 5.41 K. The abrupt shifts in the Weddell Sea not only occur at lower levels of global warming but also shows more abrupt shifts in sea ice concentration than the Amundsen and Ross Sea, occurring in 10 models compared to 5.

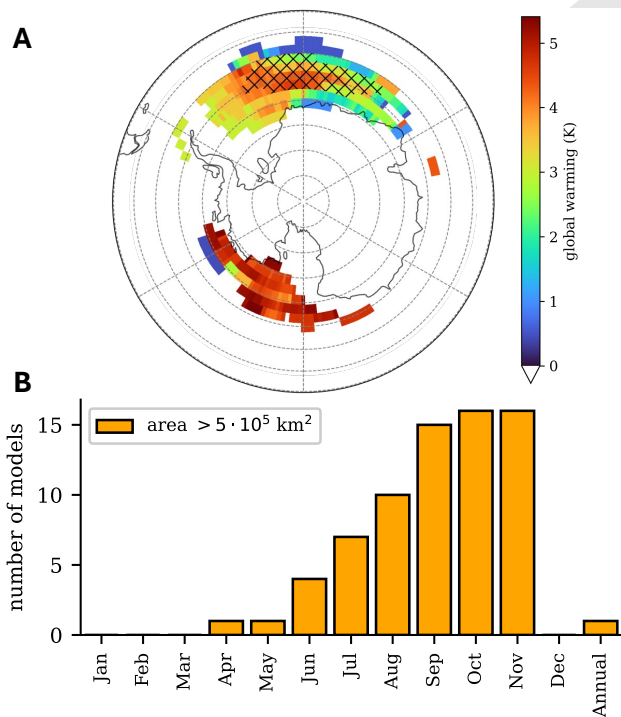


**Fig. 4. Abrupt shifts in Antarctic sea ice.** (A) The spatial distribution of the global warming level at which large-scale abrupt shifts occur in Antarctic sea ice concentration. The hashed overlay indicates that in that grid cell, at least 5 models show an abrupt shift. There is one cluster located around the Weddell Sea, and one around the Amundsen and Ross Seas. The first cluster generally experiences abrupt shifts at lower levels of global warming than the second cluster. (B) The number of models that have at least one abrupt shift larger than the given area threshold for each month.

## Subsystems not identified as tipping elements.

**Arctic Summer & Winter Sea Ice.** Arctic sea ice is often divided according to the season into summer and winter sea ice. Arctic sea ice coverage reaches its minimum extent in September. The GTP (17) classifies Arctic summer sea ice as neither a tipping element nor a system that can undergo an abrupt shift, with high confidence. This is because the melting of Arctic summer sea ice is thought to be a threshold-free process, lacking a self-reinforcing mechanism that accelerates melting beyond control once it crosses a critical threshold. Arctic sea ice coverage reaches its maximum extent in March. Winter sea ice is classified as not being a tipping element with medium confidence by the GTP (17). However, it is expected with high confidence, in contrast to the Arctic summer sea ice, that a part of the Arctic winter sea ice can disappear abruptly due to the geometry of ice thickness (32). For the summer sea ice, we analyzed August, September and October, since the minimum extent is seen in September (33), while for the winter, we analyzed February, March and April, since the maximum extent is in March (33). We took two months around the standard months to report summer and winter sea ice since the maximum and minimum might vary slightly depending on the particular model and the global warming level. In the Arctic summer sea ice, 44 out of 53 CMIP6 models show an abrupt shift, with 15 models displaying a large-scale abrupt shift. For sea ice concentration, 11 models show large-scale abrupt shifts with the onset between 1.12 and 3.13 K of global warming (90% IPR) (see Figure 2H for an example). In the Arctic winter sea ice, 48 out of 53 CMIP6 models show an abrupt shift, with 14 models displaying a large-scale abrupt shift. In sea ice concentration, 13 models show large-scale abrupt shifts, with the onset between 3.41 and 5.50 K of global warming (90% IPR) (see Figure 2I for an example).

When taking into account the other scanned variables (see Table 1), as also displayed in Figure 1B, the onset of large-scale abrupt shifts occurs between 1.04 and 4.58 K of global warming (90% IPR) for summer and between 3.28 and 5.41 K of global warming (90% IPR) for winter. For summer, 3 models have a large-scale abrupt shift in near-surface air temperature occurring between 1.49 and 4.76 K of global warming (90% IPR), which is higher than the interval for sea ice concentration. However, these 3 models do not show large-scale abrupt shifts in sea ice concentration.

Figure 5A shows the spatial distribution of the onset of large-scale abrupt shifts in terms of global warming for Arctic summer sea ice. Shown per grid cell is the average level of global warming at which these abrupt shifts occur in different models. Figure 5B shows the same but for Arctic winter sea ice. The abrupt shifts in winter occur over a larger area than in summer, which is to be expected since winter sea ice has a larger extent than summer sea ice.

When considering all months of the year, not only do we see a clear difference between summer and winter, but also a difference between the occurrence of abrupt shifts at the minimum versus maximum extent of sea ice. Figure 5C shows that from August until November there is a lower onset of



abrupt shifts than in December until June. This division corresponds to those months belonging to the group of minimum extent versus maximum extent of sea ice (below or above the average maximum and minimum extent in historical context in CMIP6 models (33)). For the minimum extent group, large-scale abrupt shifts occur between 1.16 and 3.40 K of global warming (90% IPR), while for the maximum extent group large-scale abrupt shifts occur between 3.09 and 5.40 K of global warming (90% IPR).

In their analysis, Drijfhout et al. (18) found 4 models where sea ice disappeared abruptly over an area larger than 4 million km<sup>2</sup>. We find that 7 models (CIESM, CMCC-CM2-SR5, CMCC-ESM2, E3SM-1-0, FIO-ESM-2-0, NESM3, and UKESM1-1-LL) have such an abrupt shift (which only occurs in January until May) with onsets between 3.21 and 5.24 K of global warming (90% IPR). Altogether, in partial contrast to the assessment of the GTP (17) (where they state that abrupt shifts are not expected in Arctic summer sea ice), the CMIP6 models show that not only the Arctic winter sea ice, but also the Arctic summer sea ice might undergo abrupt shifts over a substantial part of the Arctic region. Whether this is indeed due to Arctic geometry, needs further study.

**Barents Sea Ice.** Barents sea ice is mostly winter sea ice located above Scandinavia and Western Russia and is therefore a subset of the overall Arctic sea ice. It is not classified as a tipping element, albeit with low confidence due to limited studies on tipping of this system (17).

We found that 43 out of 53 models show an abrupt shift in the Barents Sea. Of these, 18 show a large-scale abrupt shift in sea ice concentration (covering an area over 0.2 million km<sup>2</sup>; Figure S7). These large-scale shifts occur between 0.49 and 2.85 K of global warming (90% IPR). There are two models with abrupt shifts covering more than 0.5 million km<sup>2</sup>: EC-Earth3-Veg and EC-Earth3-Veg-LR occurring between 1.16 and 1.30 K of global warming (see Figure 2J for EC-Earth3-Veg time series). Figure 5D shows the spatial distribution of global warming levels at which the large-scale abrupt shifts occur in sea ice concentration. The abrupt shifts are most prevalent in the northern and eastern part and less towards the south. This is likely because not all models have sea ice extended close to Northern Scandinavia.

In summary, we find evidence that Barents sea ice can undergo abrupt shifts according to the CMIP6 models. Some of the shifts we find here are part of larger shifts in Arctic sea ice since they belong to larger connected components. We only considered the parts of the bigger components that fell within the Barents Sea.

## Discussion

We assessed the presence of abrupt shifts in the CMIP6 model ensemble. For this, we used edge detection, a method to identify and quantify abrupt shifts in various climate subsystems. The majority of models (48 out of 57) have a large-scale abrupt shift in at least one of the studied systems. There is a large diversity in how many abrupt shifts the models show, indicating that some models are more prone to abrupt

shifts than others.

We detected at least one abrupt shift in all climate subsystems we examined, although the number of occurrences of these shifts vary greatly between subsystems. In the monsoon systems, we only found abrupt shifts in one model for the Indian Summer Monsoon and none for the South American and West African Monsoons. For the Indian summer monsoon, previous work (34) suggests linearly increasing rainfall with rising global temperatures under the SSP5-8.5 scenario in CMIP6 models (when averaged across the entire monsoon region). Similarly, no abrupt shifts in the monsoons were found in the CMIP5 ensemble (18). As in this study, we detected only one model with (local) abrupt shifts in just one of the monsoon systems, based on the CMIP6 models we consider abrupt shifts unlikely to occur in the monsoons.

In the sea ice systems, we detect more shifts in the Arctic than in the Antarctic region. 11 models had a large-scale abrupt shift in Antarctic sea ice concentration occurring between 0.55 and 5.41 K (90% IPR) of global warming. This is a wider range than reported by McKay et al. (6) who estimated a range of 1.4 to 2.9 K.

The GTP (17) states that Arctic summer sea ice is not a tipping element, nor is it expected to disappear abruptly. However, we found that large-scale abrupt shifts do occur in Arctic summer sea ice. For the sea ice concentration, 17 models have a large-scale abrupt shift occurring between 1.12 and 3.13 K (90% IPR) of global warming. This range is similar to the estimated range of 1.3 to 2.9 K by McKay et al. (6). However, when including all key variables, our range is between 1.04 and 4.58 K (90% IPR). This increase in range is largely caused by the abrupt shifts in near-surface air temperature and surface downwelling radiation which occur at relatively high levels of global warming in the cases we detected. The abrupt shifts in sea ice are possibly due to the increase in natural variability once sea ice retreats, thus observing synchronized retreats of sea ice due to internal variability (35).

For the Arctic winter sea ice concentration, 21 models have a large-scale abrupt shift between 3.41 and 5.50 K (90% IPR) of global warming. This range is lower than 4.5 to 8.7 K as estimated by McKay et al. (6). One possible reason for the lower upper bound of the temperature thresholds is that most CMIP6 models do not reach a global warming level of 8.7 K in the 1pctCO2 scenario. Including all key variables, this range does shift only little to 3.28 and 5.41 K (90% IPR). Finally, 18 models have a large-scale abrupt shift for the Barents sea ice concentration, occurring between 0.49 and 2.85 K (90% IPR) of global warming which is a wider range than estimated by McKay et al. (6) who place it between 1.5 to 1.7 K.

In the two vegetation systems we analyzed, the Amazon rainforest and the Boreal forest, we detected abrupt shifts in various variables. However, the edge detection, with the settings we used, performed less well on vegetation-related variables. This is due to both the low variability in many of these variables and that vegetation tends to respond over longer timescales than the decade-long timescale used with the edge detection. In general, we find numerous, discon-

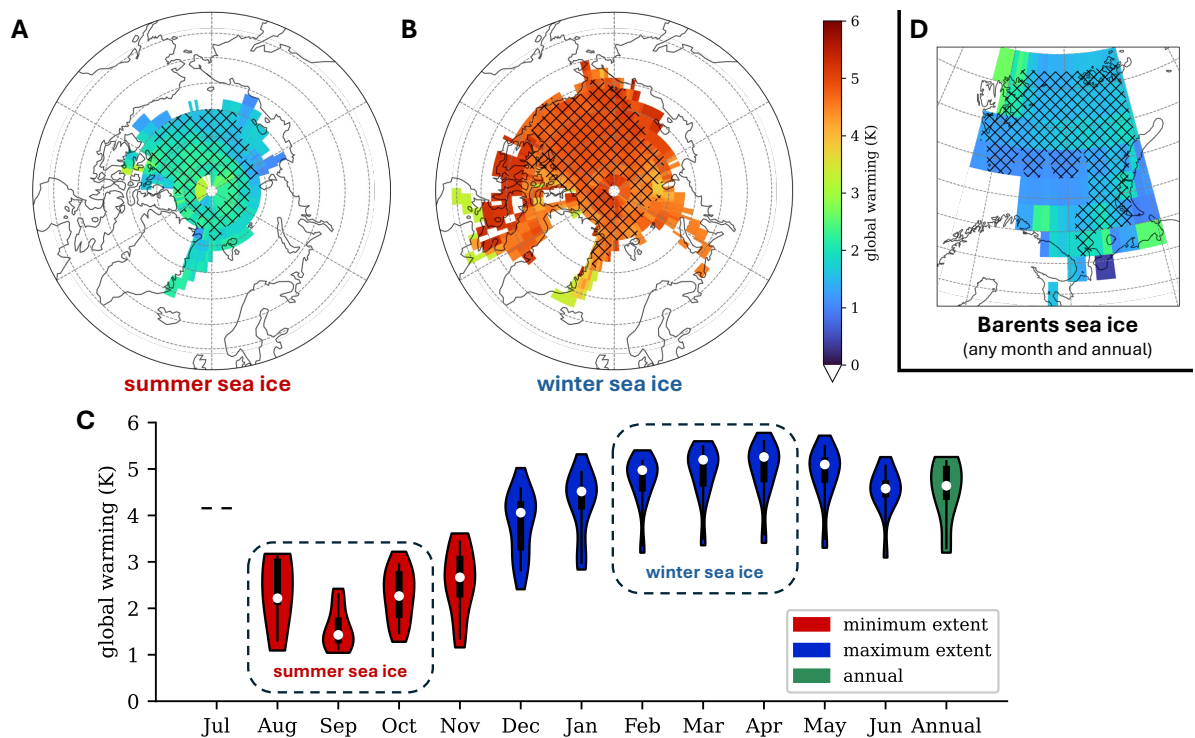


**Fig. 5. Spatial and temporal occurrence of abrupt shifts of Arctic sea ice.** (A) The spatial distribution of the global warming level at which large-scale abrupt shifts occur in Arctic summer sea ice (defined as sea ice extent in August, September, and October), (B) the spatial distribution for Arctic winter sea ice (defined as sea ice extent in February, March, and April), and (D) the spatial distribution for Barents sea ice. The hashed overlays indicates that in that grid cell at least 5 models show an abrupt shift. (C) The distribution of global warming levels at which large-scale abrupt shifts occur in the Arctic sea ice per month. The red violin plots correspond to sea ice of minimum extent, the blue violin plots show the sea ice of maximum extent, and the green violin plot the annual sea ice. There is only one model with a large-scale abrupt shift in July. The white dots show the mean, the thick black lines show the 50% interpercentile range (IPR), and the thin black lines the 90% IPR.

nected, abrupt shifts occurring over a wide range of global warming levels ranging between 0.80 and 4.87 K (90% IPR).

In the Tibetan Plateau, we detected abrupt shifts in snow-related variables in several CMIP6 models. These shifts are most prevalent in surface upwelling shortwave radiation, a proxy for albedo, indicating a sudden loss of snow cover, with 12 models showing an abrupt shift. Additionally, we found abrupt shifts in snow area percentage (4 models), melt rate (2 models), and snow depth (6 models). Drijfhout et al. (18) also identified two CMIP5 models with an abrupt decline in snow cover of the Tibetan Plateau. The level of global warming at which all these shifts occur in CMIP6 is between 0.53 and 2.61 K (90% IPR). This range overlaps with the global warming threshold estimated by McKay et al. (6), who place it between 1.4 and 2.2 K of global warming, although we also detect abrupt shifts below their lower bound of 1.4 K. Glacier tipping points could not be assessed due to their lack of representation in CMIP models, thus we were not able to fully assess the tipping potential of the Tibetan Plateau. Nevertheless, the presence of abrupt shifts in snow cover is clear in both CMIP5 and CMIP6 models.

For the land permafrost, we found more abrupt shifts than Drijfhout et al. (18) who found only one: an abrupt shift in total soil moisture content in HadGEM2-ES. However, the CMIP6 variant of this model was excluded from our analysis due to not having the simulation output available (see SI Text S1.C). The abrupt shifts detected in CMIP6, although generally individually small, add up to larger areas. For soil frozen

water content, we found only one model with an individual abrupt shift covering more than 1 million km<sup>2</sup>, but 19 models have a total area of abrupt shifts of more than 1 million km<sup>2</sup>. These occur between 0.63 and 4.59 K of global warming. This is a lower range than the global warming threshold estimated by McKay et al. (6) who place it between 3.0 and 6.0 K of global warming.

Overall, our results support previous assessments indicating that multiple climate subsystems might undergo abrupt shifts (6, 17, 18, 20). However, the level of global warming at which these shifts occur remains highly uncertain. Notably, we find the lower bound of the global warming thresholds for the North Atlantic subpolar gyre, Tibetan Plateau, Antarctic sea ice, and Arctic winter sea ice is lower in our assessment than in that of McKay et al. (6). It is important to note that their assessment was based not only on CMIP models but also on other literature, thus consisting of multiple lines of evidence. Table S4 provides an overview of the global warming thresholds from our assessment, Drijfhout et al. (18), and McKay et al. (6).

The high uncertainty in global warming levels at which abrupt shifts occur in CMIP6 models has multiple causes. One contributing factor is the grouping of shifts across different months. In some systems, abrupt shifts can occur in different months and at different levels of global warming, often depending on the season during which the shift takes place. This is evident with the Arctic sea ice, where there is a significant difference in the onset of abrupt shifts be-

tween summer and winter. However, seasonal variation alone does not fully account for the substantial differences between models. Other contributing factors include the different ways each model resolves the underlying physics and the diversity in climate sensitivity across the models.

In addition to the variation in the timing of abrupt shifts across different models and variables, this study’s estimates of global warming levels at which these shifts occur might be overestimated. The 1pctCO2 scenario represents a high forcing scenario with rapidly increasing CO<sub>2</sub> levels. Due to this rapid increase, the edge detector may identify abrupt shifts at higher warming levels than it would under a more gradual increase, as systems require time to adjust to rising CO<sub>2</sub> levels. However, the high rate of warming might also trigger rate-dependent tipping, where the system is forced into a new state due to the rate of forcing. As a result, some estimates of the global warming levels required to trigger abrupt shifts might be underestimated compared to those from scenarios with slower forcing rates, more closely aligned with the current rate of global warming.

To detect the abrupt shifts, we made several methodological choices, though alternative approaches are possible. Most importantly, the definition of the threshold for the spatial extent of large-scale abrupt shifts remains somewhat subjective, even though we based it on the specific characteristics of each subsystem. Our field lacks an objective definition of how large an abrupt shift must be to be considered relevant since its impact can be measured from multiple perspectives—for example, its effect on other climate subsystems, dependent ecosystems, or socio-economic systems.

Detecting abrupt shifts in a systematic way remains challenging given the extensive and diverse model outputs from CMIP6. Here, we use edge detection, a general tool that can be applied to all systems without requiring system-specific knowledge. However, designing a measure to quantify abruptness while avoiding detecting abrupt shifts of small magnitude remains challenging, as different variables exhibit different noise characteristics and shifts occur on different scales.

Overall, we find evidence of abrupt shifts in many climate subsystems within CMIP6. The number and onset of abrupt shifts vary significantly between models. Still, these results should be interpreted as not including all potential abrupt shifts, given that the 1pctCO2 scenario we studied has a relatively short simulation time of 150 years and does not include some important tipping elements, such as ice sheets. Longer simulations that include all climate subsystems are needed for a more accurate assessment of the long-term evolution of tipping elements under climate change. Despite these limitations, our analysis shows that higher levels of global warming increase the risk of abrupt shifts. Our estimates of uncertainty ranges of the timing of abrupt shifts generally overlap with the estimates of McKay et al. (2022), although it is important to note that they look at tipping points and not just abrupt shifts in each system. Furthermore, many of the abrupt shifts we detected, occur only over parts of a subsystem and does not always imply a full collapse of a complete subsystem.

The climate subsystems that we included in our analysis and were previously shown to have abrupt shifts in CMIP5, also showed abrupt shifts in CMIP6 (18). Even at a global warming of 1.5 K, six out of the ten subsystems studied here show a risk of large-scale abrupt shifts.

## Materials and Methods

We searched for abrupt shifts in 57 CMIP6 models run under the 1pctCO2 scenario for a total of 82 different variables with monthly frequency (see Table S3 for the full list of models). Simulations were selected based on their availability at the CMIP6 archive of the Earth System Grid Federation (ESGF) (36).

To detect abrupt shifts, we used Canny edge detection (21), as extended by Bathiany et al. (20) for climate data in many dimensions. Here, we use two spatial dimensions and one temporal dimension. For a full derivation of the underlying method, we refer the reader to (21). Since we used the edge detection method as implemented by Bathiany et al. (20), we only provide an overview of the method here. For a complete discussion and implementation details of the edge detector, please refer to SI Text S1 and Bathiany et al. (20). The relevant parameters are given in Table S1.

The edge detector requires both the *1pctCO2* and *piControl* (pre-industrial CO<sub>2</sub> levels) simulations. During preprocessing, the data is regridded to a rectilinear grid, and a Gaussian filter is applied to enhance the signal-to-noise ratio (20). The edge detector is then applied to each month and to the annual time series of the *1pctCO2* simulation. The edge detector first calculates space-time gradients using the Sobel operator, retaining only locally maximum gradients (non-maximum suppression). Hysteresis thresholding is then applied to identify *strong edges* and discard insignificant events (those below a lower threshold or not connected to a *strong edge*). The *piControl* simulation is used as a baseline for internal variance, with hysteresis thresholds set at 95% (upper) and 50% (lower) of the maximum signal.

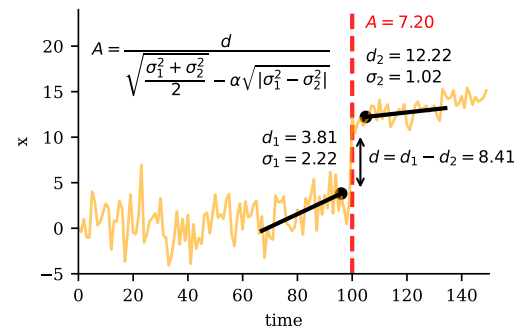


**Fig. 6. Construction of the abruptness measure.** The data shown comes from a Gaussian process with a step increase of 10 units at 100 time units where the red dashed line denotes the edge with the corresponding abruptness value  $A$ . The abruptness is calculated with Equation 1 with  $d$  the distance between the two black points  $d_1$  and  $d_2$  and the standard deviations of the black segments  $\sigma_1$  and  $\sigma_2$ . The asymmetric noise correction term is parameterized by the parameter  $\alpha = 0.4$ .

Abrupt shifts are defined as edges with a high value for the abruptness. To determine abruptness, we used an adjusted Cohen’s D as a metric for effect size, replacing the Cohen’s D

used by Bathiany et al. (20, 37). Figure 6 illustrates how the abruptness measure  $A$  was calculated from the time series. Two segments of the time series, each with a length up to  $c_{\max}$ , were extracted on either side of the edge, with a gap of  $c_{\text{trans}}$  between them. If either segment was shorter than  $c_{\min}$ , the edge was discarded due to insufficient data for accurate calculation. The abruptness measure is then defined as

$$A = \frac{d}{\sqrt{\frac{\sigma_1^2 + \sigma_2^2}{2}} - \alpha \sqrt{|\sigma_1^2 - \sigma_2^2|}}, \quad (1)$$

with  $\sigma_1$  and  $\sigma_2$  the standard deviations of the two segments. The term following  $\alpha$  is an adjustment to better detect abrupt shifts with large differences in variability before and after the shift. The optimal value of  $\alpha$  was determined through various test cases to minimize the number of false positives (see Figure S1). We set  $\alpha = 0.4$  for the analysis.

The abruptness measure quantifies the size of a shift relative to internal variability. We kept only those abrupt shifts for which the abruptness was higher than 4. When the variance before and after the edge is equal, this is equivalent to stating that the abrupt shift is greater than 4 times the standard deviation, a criterion also used by Drijfhout et al. (18) to define abrupt shifts.

**Connected Components.** To make statements regarding the spatial extent of abrupt shifts and to facilitate comparison with Drijfhout et al. (18), we applied a connected component algorithm to the edges, allowing us to obtain connected regions that experience an abrupt shift simultaneously. The algorithm consists of two steps. In the first step, small gaps in both the temporal and spatial dimensions are closed, connecting separate events that are relatively close. This step is crucial to avoid identifying numerous disconnected abrupt shifts. In the second step, the connected components are found by scanning surrounding cells in space and time for adjacent edges, grouping them into cohesive regions. The implementation details of this method can be found in SI Text S1.B1.

To verify whether the connected components still undergo an abrupt shift, we calculated the spatially weighted mean of the variable in question for these regions. We then performed a one-dimensional edge detection to identify the timing of the abrupt shift (see SI Text S1.A.1 for the algorithm of the one-dimensional edge detector, which is a simplified version of the three-dimensional edge detector). Using the same threshold as before, we classify a shift as abrupt if the abruptness exceeds 4. The area covered by the connected component is then used to determine whether the shift is large-scale. This area threshold varies for each system we study and is summarized in Table 1.

**Onset of abrupt shifts measured by global warming level.** Abrupt shifts occur in different years across the simulations, making it difficult to compare models over the same time interval as each model has a different TCR. To address this, we used the level of global warming at the edges to compare the different models. We determined the global warm-

ing level in each model by calculating the difference between the 10-year smoothed yearly mean time series of near-surface air temperature from the *IpctCO2* scenario and the *piControl* simulation.

#### ACKNOWLEDGEMENTS

This publication is part of the project 'Interacting climate tipping elements: When does tipping cause tipping?' (with project number VI.C.202.081 of the NWO Talent programme) financed by the Dutch Research Council (NWO). This is ClimTip contribution #15; the ClimTip project has received funding from the European Union's Horizon Europe research and innovation programme under grant agreement No. 101137601.

#### AUTHOR CONTRIBUTIONS

Conceptualization: ST, HD, AvdH. Formal analysis: ST. Investigation: ST. Resources: AvdH. Data curation: ST. Writing – Original Draft: ST, SF, AvdH. Writing – Review & Editing: ST, SF, RB, SB, HD, AvdH. Visualization: ST. Supervision: RB, HD, AvdH. Funding acquisition: AvdH.

#### CONFLICT OF INTEREST

The authors declare that they have no conflict of interest.

## Bibliography

- Céline Bellard, Cleo Bertelsmeier, Paul Leadley, Wilfried Thuiller, and Franck Courchamp. Impacts of climate change on the future of biodiversity. *Ecology Letters*, 15(4):365–377, 2012. ISSN 1461-0248. doi: 10.1111/j.1461-0248.2011.01736.x.
- Denis Vasiliev and Sarah Greenwood. The role of climate change in pollinator decline across the Northern Hemisphere is underestimated. *Science of The Total Environment*, 775:145788, June 2021. ISSN 0048-9697. doi: 10.1016/j.scitotenv.2021.145788.
- John W. Day, Robert R. Christian, Donald M. Boesch, Alejandro Yáñez-Arancibia, James Morris, Robert R. Twilley, Larissa Naylor, Linda Schaffner, and Court Stevenson. Consequences of Climate Change on the Ecogeomorphology of Coastal Wetlands. *Estuaries and Coasts*, 31(3):477–491, July 2008. ISSN 1559-2731. doi: 10.1007/s12237-008-9047-6.
- S. I. Seneviratne, X. Zhang, M. Adnan, W. Badi, C. Dereczynski, A. Di Luca, S. Ghosh, I. Iskandar, J. Kossin, S. Lewis, F. Otto, I. Pinto, M. Satoh, S. M. Vicente-Serrano, M. Wehner, B. Zhou, and Richard Allan. Weather and climate extreme events in a changing climate. In V. P. Masson-Delmotte, A. Zhai, S. L. Pirani, and C. Connors, editors, *Climate Change 2021: The Physical Science Basis: Working Group I contribution to the Sixth Assessment Report of the Intergovernmental Panel on Climate Change*, pages 1513–1766. Cambridge University Press, Cambridge, UK, 2021. ISBN 978-1-00-915789-6.
- Intergovernmental Panel On Climate Change. *Climate Change 2021 – The Physical Science Basis: Working Group I Contribution to the Sixth Assessment Report of the Intergovernmental Panel on Climate Change*. Cambridge University Press, 1 edition, July 2023. ISBN 978-1-00-915789-6. doi: 10.1017/9781009157896.
- David I. Armstrong McKay, Arie Staal, Jesse F. Abrams, Ricarda Winkelmann, Boris Sakschewski, Sina Loriani, Ingo Fetzer, Sarah E. Cornell, Johan Rockström, and Timothy M. Lenton. Exceeding 1.5°C global warming could trigger multiple climate tipping points. *Science*, 377(6611):eabn7950, September 2022. doi: 10.1126/science.abn7950.
- Timothy M. Lenton, Hermann Held, Elmar Kriegler, Jim W. Hall, Wolfgang Lucht, Stefan Rahmstorf, and Hans Joachim Schellnhuber. Tipping elements in the Earth's climate system. *Proceedings of the National Academy of Sciences*, 105(6):1786–1793, February 2008. doi: 10.1073/pnas.0705414105.
- Dennis Höning, Matteo Willeit, Reinhard Calov, Volker Klemann, Meike Bagge, and Andrey Ganopolski. Multistability and Transient Response of the Greenland Ice Sheet to Anthropogenic CO<sub>2</sub> Emissions. *Geophysical Research Letters*, 50(6):e2022GL101827, 2023. ISSN 1944-8007. doi: 10.1029/2022GL101827.
- René M. van Westen and Henk A. Dijkstra. Asymmetry of AMOC Hysteresis in a State-Of-The-Art Global Climate Model. *Geophysical Research Letters*, 50(22):e2023GL106088, 2023. ISSN 1944-8007. doi: 10.1029/2023GL106088.
- Didier Swingedouw, Adrien Bily, Claire Esquerdo, Leonard F. Borchert, Giovanni Sgubin, Juliette Mignot, and Matthew Menary. On the risk of abrupt changes in the North Atlantic subpolar gyre in CMIP6 models. *Annals of the New York Academy of Sciences*, 1504(1): 187–201, 2021. ISSN 1749-6632. doi: 10.1111/nyas.14659.
- W. Dansgaard, S. J. Johnsen, H. B. Clausen, D. Dahl-Jensen, N. S. Gundestrup, C. U. Hammer, C. S. Hvidberg, J. P. Steffensen, A. E. Sveinbjörnsdottir, J. Jouzel, and G. Bond. Evidence for general instability of past climate from a 250-kyr ice-core record. *Nature*, 364(6434):218–220, July 1993. ISSN 1476-4687. doi: 10.1038/364218a0.
- Nico Wunderling, Anna S. von der Heydt, Yevgeny Aksenov, Stephen Barker, Robbin Bastiaansen, Victor Brovkin, Maura Brunetti, Victor Couplet, Thomas Kleinen, Caroline H. Lear, Johannes Lohmann, Rosa María Roman-Cuesta, Sacha Sinet, Didier Swingedouw, Ricarda Winkelmann, Pallavi Anand, Jonathan Barichivich, Sebastian Bathiany, Mara Baudena, John T. Bruun, Cristiano M. Chiessi, Helen K. Coxall, David Docquier, Jonathan F. Donges, Swinda K. J. Falkena, Ann Kristin Klose, David Obura, Juan Rocha, Stefanie Rynders, Norman Julius Steinert, and Matteo Willeit. Climate tipping point interactions and cascades: a review. *Earth System Dynamics*, 15(1):41–74, January 2024. ISSN 2190-4979. doi: 10.5194/esd-15-41-2024.
- L. G. Henry, J. F. McManus, W. B. Curry, N. L. Roberts, A. M. Piotrowski, and L. D. Keigwin. North Atlantic ocean circulation and abrupt climate change during the last glaciation. *Science*, 353(6298):470–474, July 2016. doi: 10.1126/science.aaf5529.
- Simon Dietz, James Rising, Thomas Stoerk, and Gernot Wagner. Economic impacts of tipping points in the climate system. *Proceedings of the National Academy of Sciences*, 118(34):e2103081118, August 2021. doi: 10.1073/pnas.2103081118.

15. Victor Brovkin, Edward Brook, John W. Williams, Sebastian Bathiany, Timothy M. Lenton, Michael Barton, Robert M. DeConto, Jonathan F. Donges, Andrey Ganopolski, Jerry McManus, Sumner Praetorius, Anne de Vernal, Ayako Abe-Ouchi, Hai Cheng, Martin Claussen, Michel Crucifix, Gilberto Gallopin, Virginia Iglesias, Darrell S. Kaufman, Thomas Kleinen, Fabrice Lambert, Sander van der Leeuw, Hannah Liddy, Marie-France Loutre, David McGee, Kira Rehfeld, Rachael Rhodes, Alistair W. R. Seddon, Martin H. Trauth, Lillian Vanderveken, and Zicheng Yu. Past abrupt changes, tipping points and cascading impacts in the Earth system. *Nature Geoscience*, 14(8):550–558, August 2021. ISSN 1752-0908. doi: 10.1038/s41561-021-00790-5.
16. Seaver Wang, Adrianna Foster, Elizabeth A. Lenz, John D. Kessler, Julienne C. Stroeve, Liana O. Anderson, Merritt Turetsky, Richard Betts, Sijia Zou, Wei Liu, William R. Boos, and Zeke Hausfather. Mechanisms and Impacts of Earth System Tipping Elements. *Reviews of Geophysics*, 61(1):e2021RG000757, 2023. ISSN 1944-9208. doi: 10.1029/2021RG000757.
17. T.M. Lenton. The Global Tipping Points Report 2023. Technical report, University of Exeter, Exeter, UK, 2023.
18. Sybren Drijfhout, Sebastian Bathiany, Claudie Beaulieu, Victor Brovkin, Martin Claussen, Chris Huntingford, Marten Scheffer, Giovanni Sgubin, and Didier Swingedouw. Catalogue of abrupt shifts in Intergovernmental Panel on Climate Change climate models. *Proceedings of the National Academy of Sciences*, 112(43), October 2015. ISSN 0027-8424, 1091-6490. doi: 10.1073/pnas.1511451112.
19. Karl E. Taylor, Ronald J. Stouffer, and Gerald A. Meehl. An Overview of CMIP5 and the Experiment Design. *Bulletin of the American Meteorological Society*, 93(4):485–498, April 2012. doi: 10.1175/BAMS-D-11-00094.1.
20. Sebastian Bathiany, Johan Hidding, and Marten Scheffer. Edge Detection Reveals Abrupt and Extreme Climate Events. *Journal of Climate*, 33(15):6399–6421, August 2020. ISSN 0894-8755, 1520-0442. doi: 10.1175/JCLI-D-19-0449.1. 3.
21. John Canny. A Computational Approach to Edge Detection. *IEEE Transactions on Pattern Analysis and Machine Intelligence*, PAMI-8(6):679–698, November 1986. ISSN 1939-3539. doi: 10.1109/TPAMI.1986.4767851. 1.
22. Veronika Eyring, Sandrine Bony, Gerald A. Meehl, Catherine A. Senior, Bjorn Stevens, Ronald J. Stouffer, and Karl E. Taylor. Overview of the Coupled Model Intercomparison Project Phase 6 (CMIP6) experimental design and organization. *Geoscientific Model Development*, 9(5):1937–1958, May 2016. ISSN 1991-959X. doi: 10.5194/gmd-9-1937-2016. Publisher: Copernicus GmbH.
23. Nils Bochov, Anna Poltronieri, Alexander Robinson, Marisa Montoya, Martin Rypdal, and Niklas Boers. Overshooting the critical threshold for the Greenland ice sheet. *Nature*, 622(7983):528–536, October 2023. ISSN 1476-4687. doi: 10.1038/s41586-023-06503-9.
24. Zeke Hausfather, Kate Marvel, Gavin A. Schmidt, John W. Nielsen-Gammon, and Mark Zelinka. Climate simulations: recognize the ‘hot model’ problem. *Nature*, 605(7908):26–29, May 2022. doi: 10.1038/d41586-022-01192-2.
25. Keywan Riahi, Detlef P. van Vuuren, Elmar Kriegler, Jae Edmonds, Brian C. O’Neill, Shinichiro Fujimori, Nico Bauer, Katherine Calvin, Rob Dellink, Oliver Fricko, Wolfgang Lutz, Alexander Popp, Jesus Crespo Cuaresma, Samir Kc, Marian Leimbach, Leiwen Jiang, Tom Kram, Shilpa Rao, Johannes Emmerling, Kristie Ebi, Tomoko Hasegawa, Petr Havlik, Florian Humpenöder, Lara Aleluia Da Silva, Steve Smith, Eike Stehfest, Valentina Bosetti, Jiyong Eom, David Gernaat, Toshihiko Masui, Joeri Rogelj, Jessica Streffer, Laurent Drouet, Volker Krey, Gunnar Luderer, Mathijs Harmsen, Kiyoshi Takahashi, Lavinia Baumstark, Jonathan C. Doelman, Mikiko Kainuma, Zbigniew Klimont, Giacomo Marangoni, Hermann Lotze-Campen, Michael Obersteiner, Andrzej Tabeau, and Massimo Tavoni. The Shared Socioeconomic Pathways and their energy, land use, and greenhouse gas emissions implications: An overview. *Global Environmental Change*, 42:153–168, January 2017. ISSN 0959-3780. doi: 10.1016/j.gloenvcha.2016.05.009.
26. Brian C. O’Neill, Claudia Tebaldi, Detlef P. van Vuuren, Veronika Eyring, Pierre Friedlingstein, George Hurtt, Reto Knutti, Elmar Kriegler, Jean-Francois Lamarque, Jason Lowe, Gerald A. Meehl, Richard Moss, Keywan Riahi, and Benjamin M. Sanderson. The Scenario Model Intercomparison Project (ScenarioMIP) for CMIP6. *Geoscientific Model Development*, 9(9):3461–3482, September 2016. ISSN 1991-959X. doi: 10.5194/gmd-9-3461-2016.
27. Guido Grosse, Benjamin M. Jones, and Christopher D. Arp. Thermokarst lakes, drainage, and drained basins. In John F. Shroder and Elsevier, editors, *Treatise on Geomorphology*, volume 8, pages 325–353. Elsevier, Amsterdam, Netherlands, 2013. doi: 10.1016/B978-0-12-374739-6.00216-5.
28. Norman J. Steinert, Matvey V. Debolskiy, Eleanor J. Burke, Félix García-Pereira, and Hanna Lee. Evaluating permafrost definitions for global permafrost area estimates in CMIP6 climate models. *Environmental Research Letters*, 19(1):014033, December 2023. ISSN 1748-9326. doi: 10.1088/1748-9326/ad10d7.
29. Isobel M. Parry, Paul D. L. Ritchie, and Peter M. Cox. Evidence of localised Amazon rainforest dieback in CMIP6 models. *Earth System Dynamics*, 13(4):1667–1675, November 2022. ISSN 2190-4979. doi: 10.5194/esd-13-1667-2022.
30. Anil K. Gupta, Som Dutt, Hai Cheng, and Raj K. Singh. Abrupt changes in Indian summer monsoon strength during the last 900 years and their linkages to socio-economic conditions in the Indian subcontinent. *Palaeogeography, Palaeoclimatology, Palaeoecology*, 536: 109347, December 2019. ISSN 0031-0182. doi: 10.1016/j.palaeo.2019.109347.
31. Anders Levermann, Jacob Schewe, Vladimir Petoukhov, and Hermann Held. Basic mechanism for abrupt monsoon transitions. *Proceedings of the National Academy of Sciences*, 106(49):20572–20577, December 2009. doi: 10.1073/pnas.0901414106.
32. S. Bathiany, D. Notz, T. Mauritsen, G. Raedel, and V. Brovkin. On the Potential for Abrupt Arctic Winter Sea Ice Loss. *Journal of Climate*, 29(7):2703–2719, April 2016. ISSN 0894-8755, 1520-0442. doi: 10.1175/JCLI-D-15-0466.1.
33. Qi Shu, Qiang Wang, Zhenya Song, Fangli Qiao, Jiechen Zhao, Min Chu, and Xinfang Li. Assessment of Sea Ice Extent in CMIP6 With Comparison to Observations and CMIP5. *Geophysical Research Letters*, 47(9):e2020GL087965, 2020. ISSN 1944-8007. doi: 10.1029/2020GL087965.
34. Anja Katzenberger, Jacob Schewe, Julia Pongratz, and Anders Levermann. Robust increase of Indian monsoon rainfall and its variability under future warming in CMIP6 models. *Earth System Dynamics*, 12(2):367–386, April 2021. ISSN 2190-4979. doi: 10.5194/esd-12-367-2021.
35. Ian Eisenman. Geographic muting of changes in the Arctic sea ice cover. *Geophysical Research Letters*, 37(16), 2010. ISSN 1944-8007. doi: 10.1029/2010GL043741.
36. Luca Cinquini, Daniel Crichton, Chris Mattmann, John Harney, Galen Shipman, Feiyi Wang, Rachana Ananthakrishnan, Neill Miller, Sebastian Denvil, Mark Morgan, Zed Po-bre, Gavin M. Bell, Charles Doutriaux, Robert Drach, Dean Williams, Philip Kershaw, Stephen Pascoe, Estanislao Gonzalez, Sandro Fiore, and Roland Schweitzer. The Earth System Grid Federation: An open infrastructure for access to distributed geospatial data. *Future Generation Computer Systems*, 36:400–417, July 2014. ISSN 0167-739X. doi: 10.1016/j.future.2013.07.002.
37. Jacob Cohen. *Statistical power analysis for the behavioral sciences*, Rev. ed. Statistical power analysis for the behavioral sciences, Rev. ed. Lawrence Erlbaum Associates, Inc, Hillsdale, NJ, US, 1977. ISBN 978-0-12-179060-8. Pages: xv, 474.

# Supporting Information for: Assessment of Abrupt Shifts in CMIP6 Models using Edge Detection

Sjoerd Terpstra<sup>a,b,✉</sup>, Swinda K.J. Falkena<sup>a</sup>, Robbin Bastiaansen<sup>a,c</sup>, Sebastian Bathiany<sup>d,e</sup>, Henk A. Dijkstra<sup>a,b</sup>, and Anna S. von der Heydt<sup>a,b</sup>

<sup>a</sup>Institute for Marine and Atmospheric research Utrecht, Utrecht University, Utrecht, The Netherlands

<sup>b</sup>Centre for Complex Systems Studies, Utrecht University, Utrecht, The Netherlands

<sup>c</sup>Mathematical Institute, Utrecht University, Utrecht, The Netherlands

<sup>d</sup>Earth System Modelling, School of Engineering and Design, Technical University of Munich, Munich, Germany

<sup>e</sup>Potsdam Institute for Climate Impact Research, Potsdam, Germany

Correspondence: [s.terpstra@uu.nl](mailto:s.terpstra@uu.nl)

## Supplementary Note 1: Extended Methods

**A. Edge Detector.** The six major steps of the edge detector are presented below. All parameter values of the edge detector are summarized in Table S1.

**Table S1.** Parameters of the edge detector.  $S_{\max}$  = maximum Sobel signal of piControl simulation.

Parameter	Value	Comment
$h_u$	95% $S_{\max}$	upper hysteresis threshold
$h_l$	50% $S_{\max}$	lower hysteresis threshold
$\sigma_t$	10 yr	temporal smoothing scale
$\sigma_x$	100 km	spatial smoothing scale
$n_t$	0 yr	temporal tapering scale
$n_x$	5 km	spatial tapering scale
$N$	50	number of tapering iterations
$c_{\text{trans}}$	3 yr	abruptness transition length
$c_{\text{min}}$	15 yr	abruptness minimum length
$c_{\text{max}}$	30 yr	abruptness maximum length
$A_{\text{threshold}}$	4	abruptness threshold

### 1. Data Preprocessing & Tapering

The edge detector requires two simulations per single realization of a variable of a model run: the *1pctCO2* simulation and the control simulation *piControl*.

The data for all variables (atmospheric, ocean and land) must be organized on a rectilinear latitude-longitude grid. All data is regridded to the corresponding atmospheric grid as specified by the near-surface air temperature data using bilinear interpolation method of the xESMF package (1).

Land and ocean variables contain missing data outside of their domains. To prevent strong edges from being detected at the ocean-land barriers, a tapering method is applied. The original data is smoothed 50 times with a Gaussian filter, so that there is a smooth transition on the ocean-land barrier. Subsequently, the original land and ocean values are returned to replace the missing data with the tapered data. This way, no edges will be detected at the ocean-land barriers.

The standard length of a *1pctCO2* simulation is 150 years. They have a 1% annual increase in  $\text{CO}_2$  compared to pre-industrial levels for 140 years. Some models continue the simulation beyond 50 years, with  $\text{CO}_2$  at the final level reached after 140 years. These additional years are discarded to keep comparisons between models fair. The last 150 years of the *piControl* simulations are used so that they are of the same length as the *1pctCO2* simulations.

Each simulation is taken through the edge detector 13 times. The edge detection is performed on the yearly averaged time series and on the time series of each 12 individual months.

### 2. Gaussian Smoothing

Before calculating the edges, the data is smoothed using a Gaussian filter to improve the signal-to-noise ratio since the edge detector is susceptible to noise (2). The longitudinal and latitudinal dimensions are smoothed with  $\sigma_x = 100\text{km}$ , and the temporal dimension with  $\sigma_t = 10\text{yr}$ .

### 3. Gradient & Sobel Calibration

The detection of edges is based on gradients. In this step, the gradient is calculated in each dimension separately using the Sobel operator. Since we are interested in detecting edges in all dimensions, the total Sobel signal is defined as

$$S = \sqrt{(\gamma(S_x + S_y))^2 + S_t^2}, \quad (1)$$

where  $x$  is the longitudinal dimension,  $y$  latitudinal dimension, and  $t$  the temporal dimension. The factor  $\gamma$  represents the calibration between the space and time signal—a high  $\gamma$  favours spatial edges and a low  $\gamma$  favours temporal edges.  $\gamma$  is set so that the 75 percentile of the signals in space and time are equal.

### 4. Nonmaximum Supression

The resulting gradient matrix (three dimensional) contains full fields of gradients. Nonmaximum suppression is then applied to thin out the potential edges. In this process, for every grid cell in the gradient matrix, we check its neighbors in the direction of the gradient. Only if the voxel value is greater than its neighbors does it get considered as a potential edge; otherwise, it is suppressed and set to zero. By keeping only the locally maximum gradient, we ensure that each potential edge is just one grid cell wide. This way, the actual edges are kept and other signals are eliminated.

### 5. Hysteresis Thresholding

The preceding step yields many edges, but many are small in magnitude, often representing minor variations or artifacts of noise. Therefore, we apply hysteresis thresholding to separate real edges with statistically insignificant events.

Hysteresis thresholding uses two thresholds instead of just one: an upper and a lower threshold. Edges with gradients exceeding the upper threshold are retained as *strong edges*, while those falling below the lower threshold are discarded (set to a gradient of zero). Edges between these two thresholds are only kept if they are connected to a strong edge. The aim is to keep only relevant edges while applying hysteresis thresholding can also help bridging minor gaps between strong edges.

The threshold values are based on the piControl simulation since they are representative for the background noise of a particular variable and model. Therefore, a strong edge should have a gradient higher than the noise level in the piControl simulation. We use an upper threshold of 95% of the maximum of the signal of the piControl simulation, and a lower threshold of 50% of the maximum signal of the piControl simulation.

### 6. Abruptness Quantification

The last step results in a variety of edges with varying magnitude of the abrupt shift. We are interested in abrupt shift that are significantly different than background noise. Therefore, we quantify the abruptness using an effect size metric based on Cohen's D. This is further described in the Materials and Methods section of the manuscript.

**A.1. One-dimensional Edge Detection.** To detect edges in one-dimensional time series, we use a one-dimensional version of the edge detector described earlier. First, Gaussian smoothing is applied. Then, the gradient is calculated using a one-dimensional Sobel operator along the time dimension. Next, non-maximum suppression and thresholding are performed with a threshold value of 0.5. The abruptness is calculated exactly the same as in the three-dimensional edge detection.

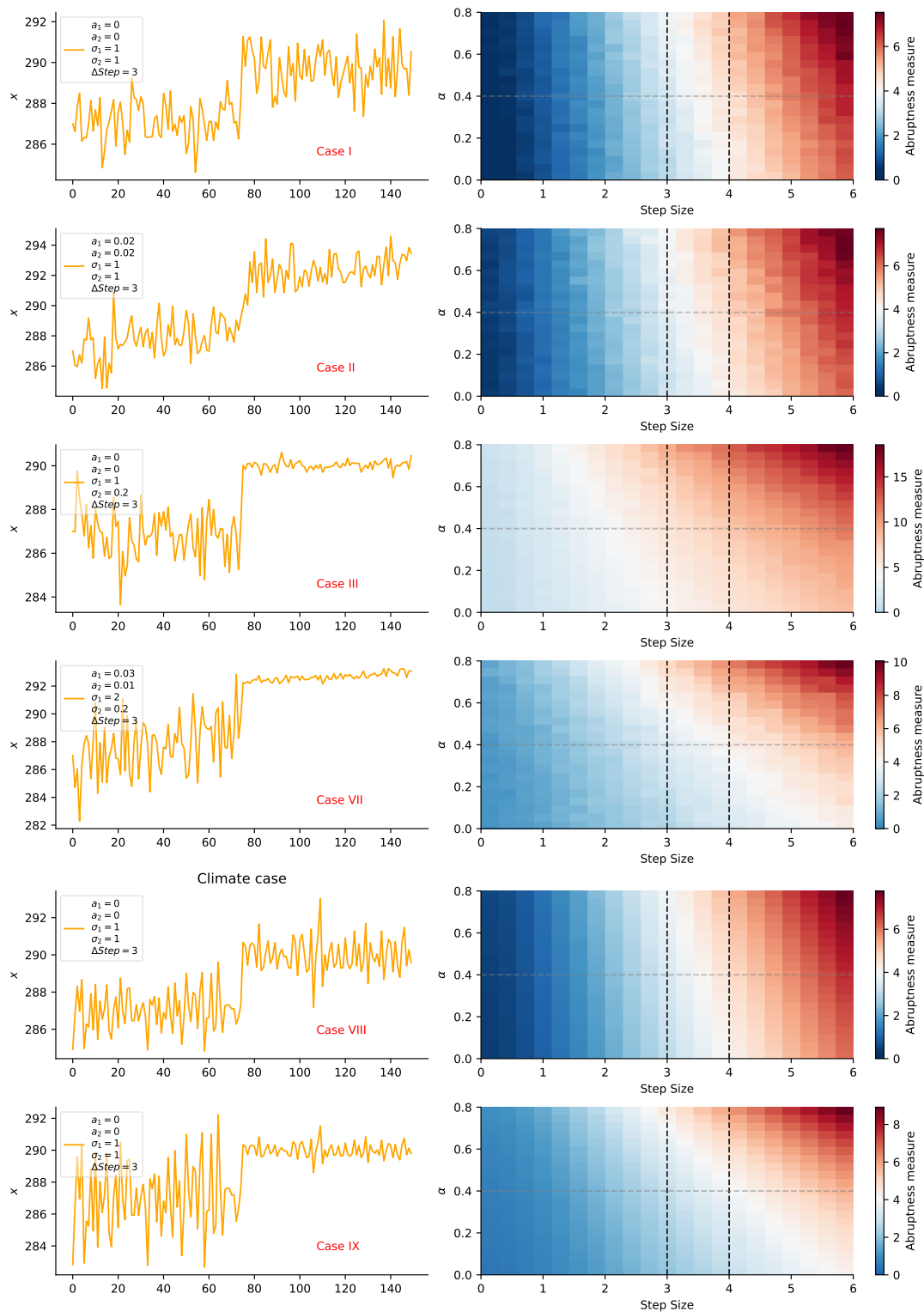


**Fig. S1. Test cases of the abruptness measure.** The measures are calculated based on 100 realizations of Gaussian processes except for the last row. Each time series has a generated abrupt change at time step 75 with a given step size. The rows correspond to separate cases of Gaussian processes with parameters specified in the legend ( $a_1$  and  $a_2$  represent the slopes of the process before and after the abrupt shift, respectively, and  $\sigma_1$  and  $\sigma_2$  represent the standard deviations before and after the abrupt shift). The last row is a realization of noise with mean 0 and standard deviation 1 of randomly selected grid cells of near-surface air temperature in a CESM2 piControl simulation. The first column shows an example time series with a step size of 3 ( $\Delta Step$ ). The second column shows heat maps for each case with the step size on the x-axis and the parameter  $\alpha$  on the y-axis. The abruptness threshold is 4 (white color).  $\alpha$  was set to 0.4 (gray dashed line) for the edge detection.



**B. Connected Components.** In order to group the abrupt shifts and make the comparison with Drijfhout et al. (3) easier, we apply a connected component algorithm to the edges to obtain connected regions that experience an abrupt shift simultaneously. This way, we can analyze bigger regions of abrupt shift and detect simultaneous tipping events more clearly. Since we work with rectilinear gridded data, we need to take into account the boundaries of the grid. The boundaries in the longitudinal direction are continuous, while the boundaries in the latitudinal direction are not treated as continuous because the exact poles miss.

As mentioned before, while abrupt shifts occur rapidly, these shifts can still span several years. We took this into account by choosing large enough smoothing scales in the edge detector. Thus, it can happen that multiple grid cells experience abrupt shifts in consecutive years, possibly with a gap. To avoid getting many disconnected abrupt shifts we choose to apply a procedure to connect loose events that are reasonably close. The same argument can be made for spatial distances. If a region undergoes a lot of abrupt shifts at the same moment with some small gaps in the spatial dimensions, it is natural to close these gaps. Therefore, our connected component analysis consists of two steps.

First, we close small gaps in the temporal and spatial dimensions. Closing is an operation to fill small holes in a given matrix through convolution. It consists of two steps: dilation and erosion. Both steps use the same convolution matrix, in our case given by the three-dimensional matrix (with a Manhattan distance of 2):

$$\text{lat} \begin{pmatrix} \begin{pmatrix} 0 & 1 & 0 \\ 1 & 1 & 1 \\ 0 & 1 & 0 \end{pmatrix} \begin{pmatrix} 1 & 1 & 1 \\ 1 & 1 & 1 \\ 1 & 1 & 1 \end{pmatrix} \begin{pmatrix} 0 & 1 & 0 \\ 1 & 1 & 1 \\ 0 & 1 & 0 \end{pmatrix} \end{pmatrix} \text{lon} \quad \text{time} \quad (2)$$

In the second step, we obtain the connected components. For this, we define a new matrix in which the middle element represents a selected edge. All other grid cells with edges that fall on the 1-values in this matrix are counted to be part of the same connected component or region. We employ depth-first search where we treat the longitudinal boundaries as continuous. We use the following three-dimensional matrix, where we include cells with an Euclidean distance smaller than 2.4:

$$\text{lat} \begin{pmatrix} \begin{pmatrix} 0 & 0 & 0 & 0 & 0 \\ 0 & 0 & 1 & 0 & 0 \\ 0 & 1 & 1 & 1 & 0 \\ 0 & 0 & 1 & 0 & 0 \\ 0 & 0 & 0 & 0 & 0 \end{pmatrix} \begin{pmatrix} 0 & 1 & 1 & 1 & 0 \\ 0 & 1 & 1 & 1 & 0 \\ 1 & 1 & 1 & 1 & 1 \\ 1 & 1 & 1 & 1 & 1 \\ 0 & 1 & 1 & 1 & 0 \end{pmatrix} \begin{pmatrix} 0 & 0 & 1 & 0 & 0 \\ 0 & 0 & 1 & 0 & 0 \\ 1 & 1 & 1 & 1 & 1 \\ 0 & 1 & 1 & 1 & 0 \\ 0 & 0 & 1 & 0 & 0 \end{pmatrix} \begin{pmatrix} 0 & 0 & 0 & 0 & 0 \\ 0 & 0 & 1 & 0 & 0 \\ 0 & 1 & 1 & 1 & 0 \\ 0 & 0 & 1 & 0 & 0 \\ 0 & 0 & 0 & 0 & 0 \end{pmatrix} \end{pmatrix} \text{lon} \quad \text{time} \quad (3)$$

It is worth noting that the precise ranges of both the closing matrix and the connected components matrix are to some degree arbitrary. There is an important trade-off to consider: if the ranges are too small, we risk having numerous disconnected regions; if they are too large, we may end up with overly connected regions that contain too many grid cells without significant edges. In the latter case, the resulting mean time series of these regions might not contain any abrupt shift anymore.

On the resulting connected components we perform multiple analyses. To check whether the regions still show tipping, we calculate the spatially weighted mean of the variable in question per region. Then, we do a one-dimensional edge detection to find the point of abrupt shift with the highest abruptness value. Using the same threshold as before, we classify a change as abrupt if the abruptness is greater than 4.

**C. Models Included & Excluded.** We analyzed the entire CMIP6 ensemble. However, we had to exclude a number of models and simulations for various reasons. First, we only included CMIP6 models that supplied the variable near-surface air temperature because it is necessary for relating simulation years to the global warming level to be able to compare the results between different models. Near-surface air temperature is a standard variable to report. Furthermore, three simulations were removed due to suspicious near-surface air temperature time series which show no continued global mean temperature increase under the high CO<sub>2</sub> forcing: GISS-E2-1-G with ensemble id r1i1p1f1 (Figure S2), CMCC-CM2-HR4 with ensemble id r1i1p1f1 (Figure S3), and GISS-E2-1-G with ensemble id r102i1p1f1 (Figure S4). We also removed ICON-ESM-LR due to an incompatible data format with the edge detector. Finally, we excluded the HadGEM models because they have different forcing for the 1pctCO2 scenario and piControl simulation: f3 for 1pctCO2 and f1 for piControl for the near-surface air temperature. Table S3 shows the models that were included in the main analysis.

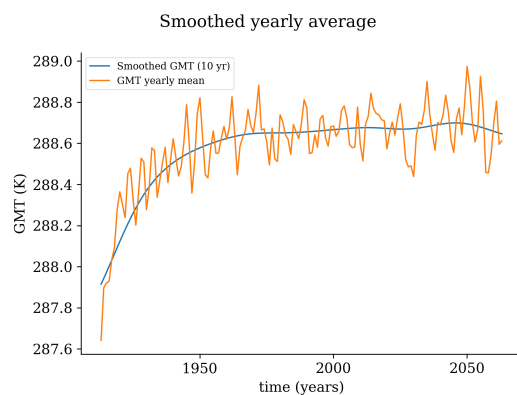


Fig. S2. Near-surface air temperature time series of CMCC-CM2-HR4, with ensemble id r1i1p1f1.

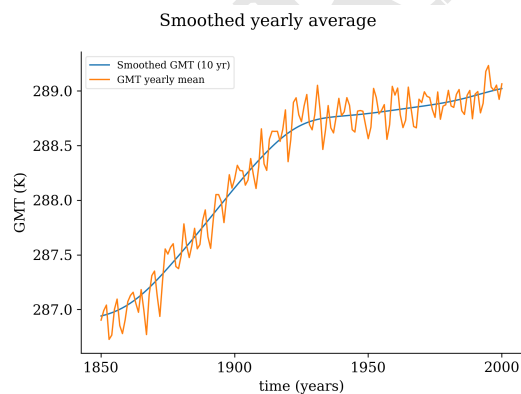


Fig. S3. Near-surface air temperature time series of GISS-E2-1-G, with ensemble id r1i1p1f1.

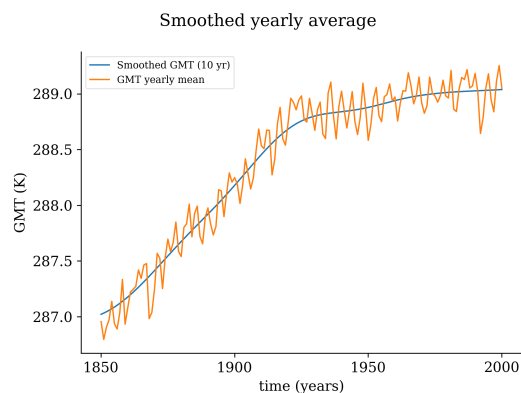


Fig. S4. Near-surface air temperature time series of GISS-E2-1-G, with ensemble id r102i1p1f1.

**D. Model Agreement.** Model agreement is defined as the fraction of models that show at least one large-scale abrupt shift in any of the relevant variables of the subsystem covering a minimum area. The total number of models on which the fraction is based on is the total number of different models that have simulations for any of the variables. By counting maximum one abrupt shift per model, we avoid correlation between different variables and counting a single event multiple times. The minimum area a large-scale abrupt shift needs to cover is given by a area threshold (where the area is based on the size of the connected component). This area threshold is defined differently per subsystem since different systems have different sizes of interest; they are given in Table 1 of the manuscript.

**E. Studied Systems.** According to the most recent review of earth system tipping elements (4), the following climate subsystems have been identified with medium to high confidence as tipping elements: the Greenland ice sheet, the West Antarctic ice sheet, marine and non-marine basins of the East Antarctic ice sheet, Mountain glaciers and land permafrost (both regional tipping elements) for the Cryosphere (Chapter 1.2 of (4)), the Amazon rainforest, Boreal forests, warm water coral reefs, mangroves and sea grass meadows as regional tipping elements for the biosphere (Chapter 1.3 of (4)), the Atlantic Meridional Overturning Circulation, the North Atlantic subpolar gyre and the Southern Ocean circulation for the atmosphere ocean system (Chapter 1.4 of (4), based on (5)). There are also a number of local scale tipping elements defined, which we do not consider here because CMIP6 models do not represent their dynamics.

In the CMIP6 models land ice sheets are not dynamically modeled, therefore we cannot study tipping behavior for the Greenland, West Antarctic, and the East Antarctic ice sheets. Of mountain glaciers, the only region that is reasonably represented in CMIP6 models is the Himalaya-Tibetan plateau, which we include as regional tipping element in our analysis. For land permafrost, most CMIP6 models include at least some land variables representing permafrost, so we included it in the analysis. A subset of the CMIP6 models includes dynamic vegetation modules (EC-Earth-Veg, GFDL-ESM4, MPI-ESM1-2-LR, NorCMP1, TaiESM1, SAM0-UNICON, and UKESM1-0-LL (6)), which allows us to investigate (for this subset of models) the Amazon rainforest and the Boreal forests dynamics to some extent. Sea grass meadows and mangroves in turn cannot be studied with CMIP6 models. Finally, out of the three tipping elements identified in atmosphere/ocean, as listed above, we investigate the subpolar gyre further. The Atlantic Meridional Overturning Circulation and Southern Ocean circulation are dependent on latitude-depth variables which are not included in our analysis.

There are also several tipping elements identified with low confidence or uncertainty, whose dynamics are represented in CMIP6 models. For these subsystems, we investigate whether there are any abrupt shifts observed in CMIP6. These are the Antarctic sea ice, the Indian summer monsoon, the West African monsoon, and the South American monsoon.

Finally, most abrupt shifts observed in CMIP6 are related to sea ice in the Northern Hemisphere. Arctic summer sea ice, Arctic winter sea ice, and Barents sea ice have not been identified as likely tipping elements. Although Arctic winter sea ice has been designated as abrupt, Arctic summer sea ice and Barents sea ice have not been designated as abrupt. However, (2) detected many edges in the Arctic region in the CMIP5 models. Therefore, we included these systems in our analysis.

**Table S2.** The 82 CMIP6 variables included in the study for atmosphere, ocean, and land.

Label	Name
<b>Atmosphere</b>	
tas	Near-surface air temperature (2m height)
ts	Surface temperature
tasmax	Daily Maximum Near-Surface Air Temperature
tasmin	Daily Minimum Near-Surface Air Temperature
hfss	Surface Upward Latent Heat Flux
hfss	Surface Upward Sensible Heat Flux
tauu	Surface Downward Eastward Wind Stress
tauv	Surface Downward Northward Wind Stress
uas	Eastward Near-Surface Wind
vas	Northward Near-Surface Wind
sfcWind	Near-Surface Wind Speed
ps	Surface Air Pressure
psl	Sea level pressure
cct	Air Pressure at Convective Cloud Top
ci	Fraction of Time Convection Occurs in Cell
sci	Fraction of Time Shallow Convection Occurs
rlut	TOA Outgoing Longwave Radiation
rsut	TOA Outgoing Shortwave Radiation
rlutcs	TOA Outgoing Clear-Sky Longwave Radiation
rsutcs	TOA Outgoing Clear-Sky Shortwave Radiation
rsds	Surface Downwelling Shortwave Radiation
rsus	Surface Upwelling Shortwave Radiation
rlus	Surface Upwelling Longwave Radiation
rlds	Surface Downwelling Longwave Radiation
rsuscs	Surface Upwelling Clear-Sky Shortwave Radiation
rsdscs	Surface Downwelling Clear-Sky Shortwave Radiation
rldscs	Surface Downwelling Clear-Sky Longwave Radiation
clt	Total cloud cover percentage
cls	Percentage Cover of Stratiform Cloud
clc	Convective Cloud Area Percentage
prc	Convective Precipitation
pr	Precipitation
prsn	Snowfall Flux
prw	Water Vapor Path
hurs	Near-Surface Relative Humidity
huss	Near-Surface Specific Humidity
clivi	Ice Water Path
clwvi	Condensed Water Path
<b>Ocean</b>	
siconc	Sea ice concentration
sidmassmeltbot	Sea-Ice Mass Change Through Bottom Melting
sidmassmelttop	Sea-Ice Mass Change Through Surface Melting
sithick	Sea ice thickness
fgco2	Gas exchange flux of CO2 (positive into ocean)
spco2	Surface Aqueous Partial Pressure of CO2
dpcO2	Delta CO2 Partial Pressure
epc100	Downward Flux of Particulate Organic Carbon
froc	Downward Organic Carbon Flux at Ocean Bottom
fric	Downward Inorganic Carbon Flux at Ocean Bottom
intdic	Dissolved Inorganic Carbon Content
intpp	Primary Organic Carbon Production by All Types of Phytoplankton
zoocos	Surface Zooplankton Carbon Concentration
thetaot	Sea Water Potential Temperature Vertically Integrated
sos	Sea Surface Salinity

hfds	Downward Heat Flux at Sea Water Surface
tos	Sea Surface Temperature
talkos	Surface Total Alkalinity
phos	Surface pH
wfo	Water Flux into Sea Water
chlos	Surface Mass Concentration of Total Phytoplankton Expressed as Chlorophyll in Sea Water
mlotst	Ocean Mixed Layer Thickness Defined by Sigma T
pbo	Sea Water Pressure at Sea Floor
zos	Sea Surface Height Above Geoid

---

Land

lai	Leaf Area Index
treeFrac	Tree Cover Percentage
grassFrac	Natural Grass Area Percentage
baresoilFrac	Bare Soil Percentage Area Coverage
mrso	Total Soil Moisture Content
mro	Total Runoff
mros	Surface Runoff
mroIs	Ice Sheet Total Runoff
snm	Surface Snow Melt
snd	Snow Depth
snc	Snow area percentage
cSoil	Carbon Mass in Model Soil Pool
cVeg	Carbon Mass in Vegetation
fFire	Carbon Mass Flux into Atmosphere Due to CO2 Emission from Fire Excluding Land-Use Change
fFireAll	Carbon Mass Flux into Atmosphere Due to CO2 Emission from Fire Including All Sources
fVegLitter	Total Carbon Mass Flux from Vegetation to Litter
fVegSoil	Total Carbon Mass Flux from Vegetation Directly to Soil
gpp	Carbon Mass Flux out of Atmosphere Due to Gross Primary Production on Land
rGrowth	Total Autotrophic Respiration on Land as Carbon Mass Flux
mrfso	Soil Frozen Water Content

---

## Supplementary Note 2: Extended Results

**A. Abrupt Shifts & ECS.** To test if the number of abrupt shifts in a model depends on its climate sensitivity, we performed a two-sided Pearson correlation test between the number of subsystems with large-scale abrupt shifts per model with the models' equilibrium climate sensitivity (ECS, model values obtained from (7, 8)). The ECS is defined as the level of global warming resulting from a doubling of CO<sub>2</sub> levels relative to preindustrial conditions until an equilibrium in global warming has been reached. We excluded the Amazon rainforest and Boreal forests as no consistent signals were detected (see the Amazon rainforest and Boreal forests sections in the manuscript). The correlation between ECS and the number of subsystems with large-scale abrupt shifts is  $r = 0.625$  with  $p < 0.001$ , meaning a significant correlation of moderate positive strength. Thus, models with high ECS generally have more large-scale abrupt shifts than models with low ECS.

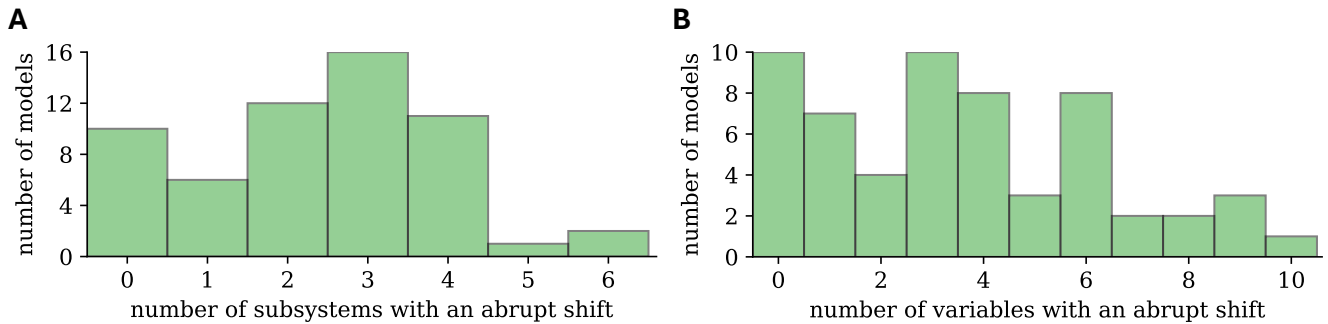


**Fig. S5. Number of models that show an abrupt shift.** Panel **A** shows the distribution of the number of subsystems with large-scale abrupt shifts across different models. The horizontal axis represents the number of subsystems with large-scale abrupt shifts, while the vertical axis indicates the number of models. Panel **B** shows the distribution of the number of with large-scale abrupt shifts across different models. The horizontal axis represents the number of variables, aggregated over the main variables of all subsystems as described in Table 1 in the manuscript, while the vertical axis indicates the number of models.

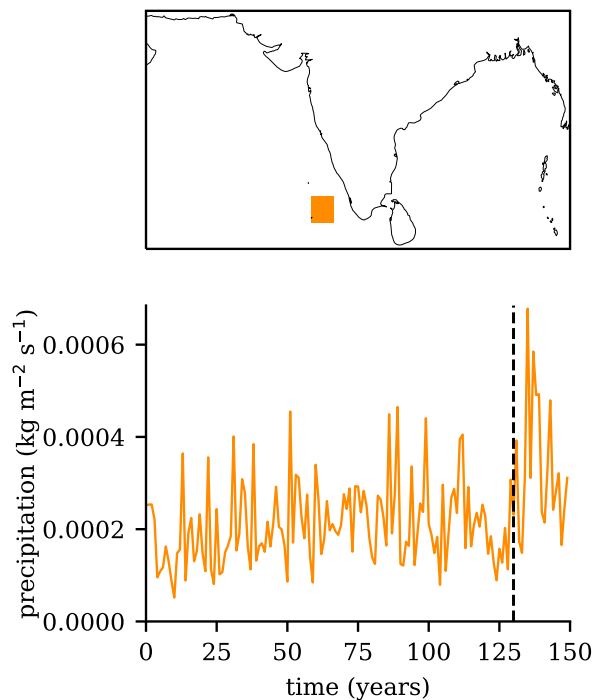


**Fig. S6. Detected abrupt shift in precipitation.** An abrupt shift is detected for the Indian summer monsoon in precipitation at the black, dashed line. Upon visual inspection, this is possibly an extreme event and not a persistent change in state.

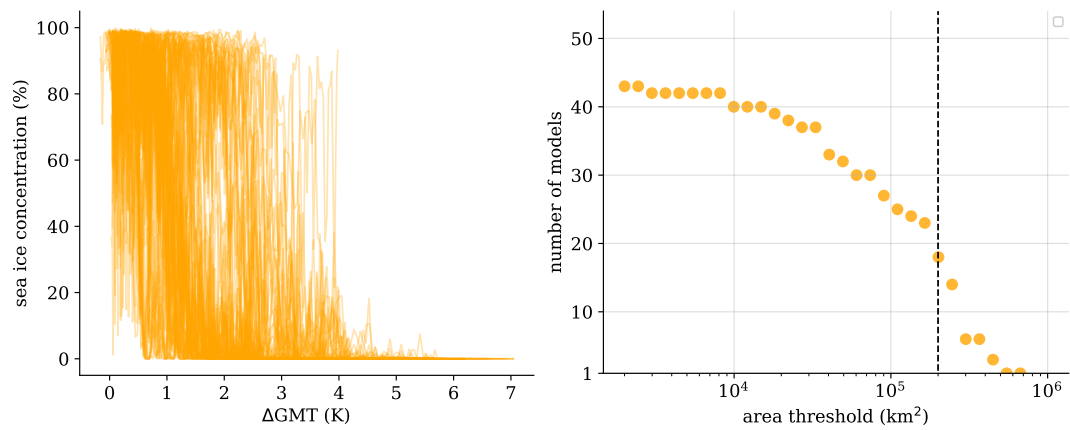


**Fig. S7. Abrupt shifts in Barents sea ice.** Panel A shows the sea ice concentration for all detected large-scale abrupt shifts, covering an area of at least  $3 \cdot 10^5 \text{ km}^2$ , versus the global warming level which increases almost linearly over time (this is used instead of time since not all models warm equally fast). Panel B shows the number of models that have at least one abrupt shift larger than a given area threshold.

**Table S3.** Subsystems with large-scale abrupt shifts per model and number of variables with large-scale abrupt shifts. SPG = North Atlantic subpolar gyre, HTP = Tibetan plateau, LPERM = land permafrost, AMAZ = Amazon rainforest, BORF = Boreal forests, ISMON = Indian summer monsoon, AntSI = Antarctic sea ice, ASSI = Arctic summer sea ice, AWSI = Arctic winter sea ice, and BARI = Barents sea ice. Here, only the key variables of each subsystem is considered, making the total number of variables 40 instead of all 82.

Model	Subsystems with large-scale abrupt shift	Number of variables with large-scale abrupt shift
ACCESS-CM2	SPG, BARI, LPERM	4
ACCESS-ESM1-5	-	
AWI-ESM-1-1-LR	HTP, ISMON	2
BCC-CSM2-MR	SPG, AntSI, LPERM	7
BCC-ESM1	SPG, AntSI, BARI, LPERM	8
CAMS-CSM1-0	LPERM	1
CAS-ESM2-0	-	
CESM2	SPG, LPERM	4
CESM2-FV2	APG, AntSI, BARI, LPERM	7
CESM2-WACCM	SPG, AntSI, LPERM	6
CESM2-WACCM-FV2	SPG, AntSI, LPERM	4
CIESM	SPG, ASSI, AWSI, BARI	4
CMCC-CM2-SR5	AWSI, LPERM	5
CMCC-ESM2	AWSI, LPERM	4
CNRM-CM6-1	SPG, AntSI	3
CNRM-CM6-1-HR	SPG, AntSI	5
CNRM-ESM2-1	SPG, AntSI, ASSI, BARI	6
CanESM5	ASSI, AWSI, BARI, HTP	6
CanESM5-1	AWSI, BARI, HTP	4
CanESM5-CanOE	ASSI, AWSI, HTP	5
E3SM-1-0	AWSI, LPERM	3
E3SM-2-0	AWSI	1
EC-Earth3	ASSI, BARI	1
EC-Earth3-AerChem	ASSI, BARI	3
EC-Earth3-Veg	SPG, ASSI, BARI, AMAZ, BORF, LPERM	13
EC-Earth3-Veg-LR	ASSI, BARI, LPERM	4
FGOALS-f3-L	SPG, BARI	3
FGOALS-g3	SPG, BARI, HTP	4
FIO-ESM-2-0	AntSI, ASSI, AWSI	3
GFDL-CM4	HTP	1
GFDL-ESM4	SPG, AMAZ, BORF	10
GISS-E2-1-H	SPG, AntSI, HTP	8
GISS-E2-2-G	SPG, HTP	4
GISS-E2-2-H	SPG, BARI, HTP, LPERM	6
IITM-ESM	SPG	1
INM-CM4-8	-	0
INM-CM5-0	-	0
IPSL-CM5A2-INCA	SPG, HTP	3
IPSL-CM6A-LR	ASSI, AWSI, HTP, LPERM	7
IPSL-CM6A-MR1	?	?
KACE-1-0-G	ASSI, BARI	2
KIOST-ESM	SPG, BARI, HTP	4
MCM-UA-1-0	-	0
MIROC-ES2L	BARI	1
MIROC6	ASSI, BARI	3
MPI-ESM-1-2-HAM	-	0
MPI-ESM1-2-HR	-	0
MPI-ESM1-2-LR	SPG, AntSI, AMAZ, BORF	8
MRI-ESM2-0	SPG, BARI	3
NESM3	AWSI, BARI	1
NorCPM1	LPERM	1
NorESM2-LM	BARI, LPERM	2



NorESM2-MM	-	0
SAM0-UNICON	SPG, AntSI, AMAZ, BORF, LPERM	9
TaiESM1	ASSI, AWSI, AMAZ, BORF, LPERM	11
UKESM1-0-LL	AntSI, ASSI, AWSI, BARI, AMAZ, BORF, LPERM	15
UKESM1-1-LL	AntSI, ASSI, AWSI, LPERM	3

---

PREPRINT

**Table S4.** Global warming thresholds (compared to pre-industrial temperatures) of each studied climate subsystems in Kelvin. For this assessment, the 90% interpercentile range of detected large-scale abrupt shifts of all key variables per subsystem (see Table 1 in manuscript) is reported, for Drijfhout et al. (3) the values at which the abrupt shifts occur, and for McKay et al. (9) the estimated range of the tipping point based on their literature review is reported. The Boreal forest southern dieback and northern expansion categories as used in McKay et al. (9) are collapsed into one category (dieback: 1.4 - 5.0 K; northern expansion: 1.5 - 7.2 K) since we do not distinguish between these two categories in our assessment.

Subsystem	This Assessment	Drijfhout et al. (2015)	McKay et al. (2022)
North Atlantic subpolar gyre	0.46 - 2.87	1.7	1.1 - 3.8
Tibetan Plateau	0.53 - 2.61	1.8	1.4 - 2.2
Land permafrost	0.97 - 3.82	5.6	3.0 - 6.0
Amazon rainforest	-	2.5/6.2	2.0 - 6.0
Boreal forests	-	-	1.4 - 7.2
Indian summer monsoon	0.76	-	-
Antarctic sea ice	0.51 - 5.27	2.1	1.4 - 2.9
Arctic summer sea ice	1.04 - 4.58	?	1.3 - 2.9
Arctic winter sea ice	3.28 - 5.41	6.3	4.5 - 8.7
Barents sea ice	0.49 - 2.99	1.6	1.5 - 1.7

PREPRINT

## Bibliography

1. Jiawei Zhuang, raphael dussin, David Huard, Pascal Bourgault, Anderson Banirirwe, Stephane Raynaud, Brewster Malevich, Martin Schupfner, Filipe, Sam Levang, Charles Gauthier, André Jüling, Mattia Almansi, RichardScottOZ, RondeauG, Stephan Rasp, Trevor James Smith, Jemma Stachelek, Matthew Plough, Pierre, Ray Bell, Romain Caneill, and Xianxiang Li. pangeo-data/xESMF: v0.8.2, September 2023.
2. Sebastian Bathiany, Johan Hidding, and Marten Scheffer. Edge Detection Reveals Abrupt and Extreme Climate Events. *Journal of Climate*, 33(15):6399–6421, August 2020. ISSN 0894-8755, 1520-0442. doi: 10.1175/JCLI-D-19-0449.1. 3.
3. Sybren Drijfhout, Sebastian Bathiany, Claudie Beaulieu, Victor Brovkin, Martin Claussen, Chris Huntingford, Marten Scheffer, Giovanni Sgubin, and Didier Swingedouw. Catalogue of abrupt shifts in Intergovernmental Panel on Climate Change climate models. *Proceedings of the National Academy of Sciences*, 112(43), October 2015. ISSN 0027-8424, 1091-6490. doi: 10.1073/pnas.1511451112.
4. T.M. Lenton. The Global Tipping Points Report 2023. Technical report, University of Exeter, Exeter, UK, 2023.
5. Sina Loriani, Yevgeny Aksenov, David Armstrong McKay, Govindasamy Bala, Andreas Born, Cristiano M. Chiessi, Henk Dijkstra, Jonathan F. Donges, Sybren Drijfhout, Matthew H. England, Alexey V. Fedorov, Laura Jackson, Kai Kornhuber, Gabriele Messori, Francesco Pausata, Stefanie Rynders, Jean-Baptiste Salée, Bablu Sinha, Steven Sherwood, Didier Swingedouw, and Thejna Tharammal. Tipping points in ocean and atmosphere circulations. *EGUsphere*, pages 1–62, December 2023. doi: 10.5194/egusphere-2023-2589.
6. Isobel M. Parry, Paul D. L. Ritchie, and Peter M. Cox. Evidence of localised Amazon rainforest dieback in CMIP6 models. *Earth System Dynamics*, 13(4):1667–1675, November 2022. ISSN 2190-4979. doi: 10.5194/esd-13-1667-2022.
7. Intergovernmental Panel On Climate Change. *Climate Change 2021 – The Physical Science Basis: Working Group I Contribution to the Sixth Assessment Report of the Intergovernmental Panel on Climate Change*. Cambridge University Press, 1 edition, July 2023. ISBN 978-1-00-915789-6. doi: 10.1017/9781009157896.
8. Zeke Hausfather, Kate Marvel, Gavin A. Schmidt, John W. Nielsen-Gammon, and Mark Zelinka. Climate simulations: recognize the ‘hot model’ problem. *Nature*, 605(7908):26–29, May 2022. doi: 10.1038/d41586-022-01192-2.
9. David I. Armstrong McKay, Arie Staal, Jesse F. Abrams, Ricarda Winkelmann, Boris Sakschewski, Sina Loriani, Ingo Fetzer, Sarah E. Cornell, Johan Rockström, and Timothy M. Lenton. Exceeding 1.5°C global warming could trigger multiple climate tipping points. *Science*, 377(6611):eabn7950, September 2022. doi: 10.1126/science.abn7950.

PREPRINT